

# Electronic transport across a junction between armchair graphene nanotube and zigzag nanoribbon

## Transmission in an armchair nanotube without a zigzag half-line of dimers

Basant Lal Sharma<sup>a</sup>

Department of Mechanical Engineering, Indian Institute of Technology Kanpur, Kanpur, U.P. 208016, India

Received 14 November 2017 / Received in final form 28 February 2018

Published online 17 May 2018 – © EDP Sciences, Società Italiana di Fisica, Springer-Verlag 2018

**Abstract.** Based on the well known nearest-neighbor tight-binding approximation for graphene, an exact expression for the electronic conductance across a zigzag nanoribbon/armchair nanotube junction is presented for non-interacting electrons. The junction results from the removal of a half-row of zigzag dimers in armchair nanotube, or equivalently by partial rolling of zigzag nanoribbon and insertion of a half-row of zigzag dimers in between. From the former point of view, a discrete form of Dirichlet condition is imposed on a zigzag half-line of dimers assuming the vanishing of wave function outside the physical structure. A closed form expression is provided for the reflection and transmission moduli for the outgoing wave modes for each given electronic wave mode incident from either side of the junction. It is demonstrated that such a contact junction between the nanotube and nanoribbon exhibits negligible backscattering, and the transmission has been found to be nearly ballistic. In contrast to the previously reported studies for partially unzipped carbon nanotubes (CNTs), using the same tight binding model, it is found that due to the “defect” there is certain amount of mixing between the electronic wave modes with even and odd reflection symmetries. But the junction remains a perfect valley filter for CNTs at certain energy ranges. Applications aside from the electronic case, include wave propagation in quasi-one-dimensional honeycomb structures of graphene-like constitution. The paper includes several numerical calculations, analytical derivations, and graphical results, which complement the provision of succinct closed form expressions.

## 1 Introduction

The last three decades have witnessed an impetuous rise in the scientific works concerning carbon nanotubes (CNTs) [1,2] and graphene nanoribbons (GNRs) [3,4]. These researches have marked their presence from the viewpoint of transport of phonons, electrons, and magnetic spins [5–7]; partly associated with geometric structure of (curved) nanotubes and (flat) nanoribbons, various edge shapes and edge-localized states [8–11]. Besides this, the photonic [12] and phononic [13] structures of similar type [14] also reveal analogous features, which has further enhanced the theoretical framework. Apart from the presence of “point” defects [15,16] in a “perfect” structure, the interface associated with junctions between GNRs with various edge shapes as well as CNTs with different chiralities and orientations is relevant for the emerging field of nanoelectronics [17–19]. Over the last decade, several experiments have shown how nanotubes can be unzipped into GNRs [20–23], to arrive at a natural junction with functional properties suitable for certain electro-magnetic devices [24,25]; for instance, devices containing mixed

graphene-nanotubes have been also recently shown [26]. This has generated a need for theoretical understanding of conductance associated with junctions between GNR and CNT structures [27–29].

In this paper, a special junction is considered for which the electronic transmission problem is shown schematically in Figure 1. A zigzag GNR is characterized by the number of zigzag dimers  $n$  across the nanoribbon width, i.e.,  $n$  zigzag chains, along with the usual convention for their nomenclature as  $n$ -zGNR. By a similar convention, an armchair nanotube is denoted by  $(n, n)$ -aCNT [15] where  $2n$  is the number of carbon atoms of CNT circumference. The junction shown in Figure 1 can be interpreted as  $(N - 1)$ -zGNR/ $(N, N)$ -aCNT junction, which is formed by partial removal of zigzag dimers from an armchair CNT, denoted by (A), so that  $n = N - 1 = 2N - 1$  for the nanoribbon on the left side, denoted by (B), of the junction; a schematic description of the construction is provided in Figures 2a and 2b. In past, several researches have appeared concerning the transport properties of GNR/zigzag-CNT junctions and GNR/aCNT junctions [24,25,28,30]. The electron transmission probability through a junction of a GNR and a metallic zigzag CNT has been calculated [28] using the nearest-neighbor

<sup>a</sup> e-mail: [bls@iitk.ac.in](mailto:bls@iitk.ac.in)

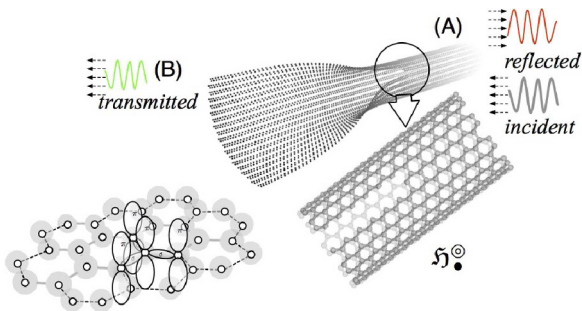


**Fig. 1.** Zigzag nanoribbon and armchair nanotube junction (see also Fig. 2a) along with a schematic illustration of  $\pi$  orbitals of graphene.

tight-binding (TB) approximation and matching the wave functions in GNR and CNT regions at the interface. In this sense, as a contrast to the study of [27,30],<sup>1</sup> there is a *defect* at the contact interface so that the CNT/GNR junction can be regarded as an unzipped CNT with an additional half line of zigzag dimers removed. Quantum effect manifests itself in the description of the confinement induced eigen-basis states, and the scattering potential gives rise to the concomitant quantum mechanical transition [32]. A cursory view of the researches is enough to realize that the usual computational approach, based on first principles [33,34], is well-complemented by an analytical, though intensive, approach in order to understand certain basic phenomenological aspects [28]. In this context, the success of the latter kinds can be traced back to around sixty years when Wallace [35] modeled the electronic band structure of graphene and carbon-like systems in general. Within simple TB theory [36,37] for graphene, several scientific leaps have been already made [8,9]. The calculations of the present paper are still based on the well-known TB model for graphene, which considers only the interaction between nearest neighbors and neglects other ones. The unzipping tantamounts to the absence of hopping between the carbon atoms where the opening occurs. Further, it is assumed that the unzipping does not modify the hopping between the neighboring carbon atoms [27]. Thus, with one  $\pi$ -electron per carbon atom (as schematically shown in left part of Fig. 1), the spinless TB Hamiltonian is assumed to approximate the electronic structure [35].

Using the experimental findings, it is known that the concept of coherent individual modes (eigen-basis states) diminishes in sufficiently long waveguides. From a theoretical point of view, it appears rational to solve the Schrödinger's equation within the tight binding

<sup>1</sup> Based on a question posed by one of the reviewers, an analytical approach on the lines of the present paper and [31] has been also applied to the electronic transmission problem across such a zigzag crack induced zGNR/aCNT junction. Preliminary investigations reveal that there exists a closed form solution of the same nature; in a forthcoming paper, adequate relevant details will be provided along with a comparison between the electronic conductance in the two structures. In contrast to the zigzag crack induced junction [27,30], there is a mixing between even and odd modes for a “double” crack studied in the present paper.

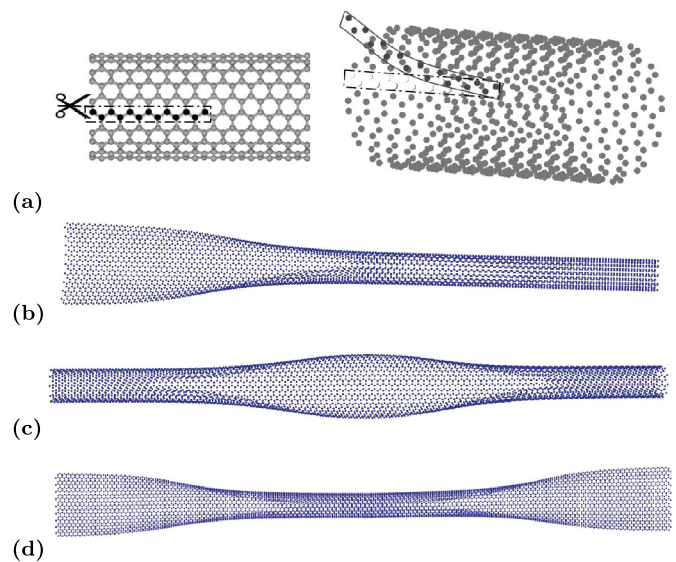


**Fig. 2.** (a) Schematic construction of a  $(N-1)$ -zGNR/ $(N,N)$ -aCNT junction by removing a zigzag half-line of dimers in nanotube. Schematic diagram of junctions between nanoribbon and nanotube: (b)  $(N-1)$ -zGNR/ $(N,N)$ -aCNT junction, (c)  $(N,N)$ -aCNT/ $(N-1)$ -zGNR/ $(N,N)$ -aCNT junction, (d)  $(N-1)$ -zGNR/ $(N,N)$ -aCNT/ $(N-1)$ -zGNR junction.

approximation by using the decomposition into the eigen-modes of the quantum waveguide in analogy to classical microwaves [38,39]. Using such “mode-matching” strategy, it is shown that a single zGNR/aCNT junction with a defect exhibits an almost perfect propagation for the electrons. The incident electronic wave from the nanoribbon, after interacting with the junction, transforms into the nanotube lead with negligible backscattering and evanescent excitation. The same conclusions are also valid for low-energy electron transport where the electron transmission is provided by propagating modes in the nanotube channel. As a point of departure from the established methods, that of Green function formalism [40], a strongly analytical approach based on complex functions [41] is followed that gives the closed form expression for the scattering amplitudes. The exact solution, as an application of the analysis of the second problem of [42], presents itself via a standard application of the Wiener–Hopf technique. The *Landauer–Büttiker formalism* (or rather a viewpoint of conduction [43,44]) provides the necessary framework for calculation of the electrical conductance from the asymptotic form of the scattering states (see Sects. 8.4.3 and 8.5.3 of [45]). Several qualitative features, earlier arrived at via numerical calculations, are given an adequate analytic description in terms of elementary functions. An important role is played by the Chebyshev polynomials throughout the paper [46,47]; recently, the same family of polynomial has been finding relevance in analysis of phenomena of similar nature [48,49]. The paper follows the notation and detailed analysis involving Chebyshev polynomials as presented by [50]. Some of the expressions stated in the paper are explicit, while others are implicit, which are provided in terms of the roots of

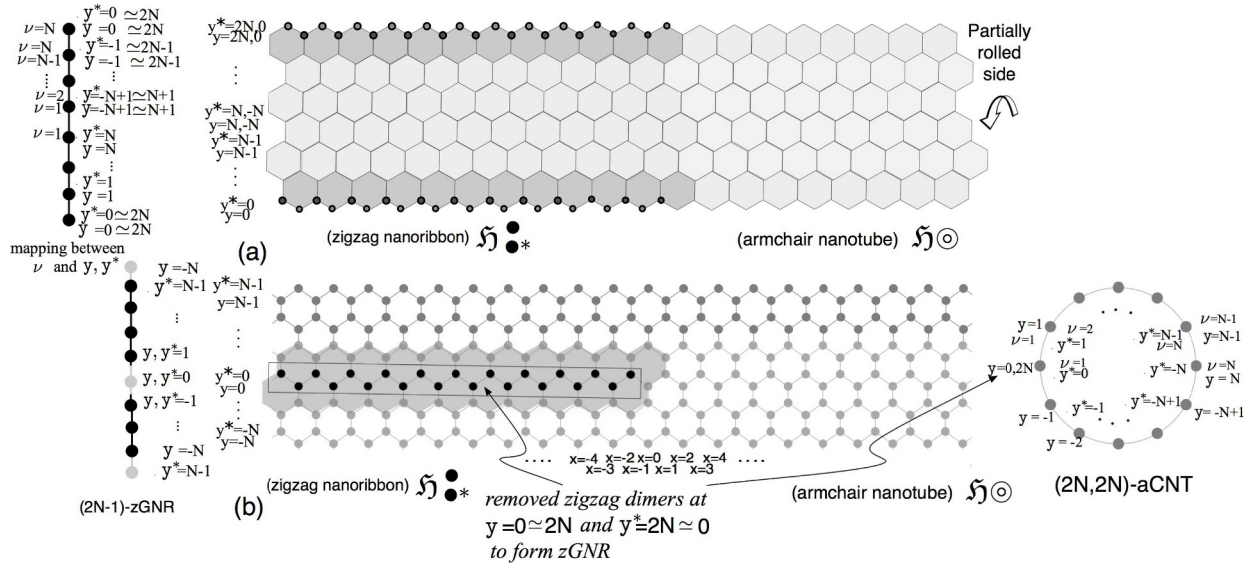


**Fig. 3.** zGNR/aCNT-junction from the point of view of the nanoribbon zGNR  $\mathfrak{H}^*$  in (a) vs. nanotube aCNT  $\mathfrak{H}^\circ$  in (b). Labels  $\nu$  for the lattice coordinates  $y, y^*$  in the context of wave modes on either side of  $\mathfrak{H}^\circ$ .

various kinds of the Chebyshev polynomials (or their linear combinations) [50]. As the main result derived in the paper, a closed form expression is obtained for the reflection and transmission moduli for the outgoing wave modes for each given electronic wave mode incident from either side of the junction (shown as (A) and (B) schematically in Fig. 1). After an application of various algebraic manipulations on the rudimentary form of the transmission and reflection moduli, it is found that there is a succinct expression that represents them. The conductance for electronic transmission has been found to be nearly ballistic, similar to the conclusions drawn by defectless junction structures analyzed by [27,28,30]. A pair of such junctions (the double junction [30]) as shown in Figure 1 leads to either  $(N, N)$ -aCNT/ $(N - 1)$ -zGNR/ $(N, N)$ -aCNT or  $(N - 1)$ -zGNR/ $(N, N)$ -aCNT/ $(N - 1)$ -zGNR junctions, respectively; also shown schematically in Figures 2c and 2d. Although the latter two geometries of the junction structure are not analyzed in this paper, the analysis can be extended using the existing framework of scattering matrices for dealing with a combination of scatterers [51,52]. In this context, the mathematical counterparts of a finite “rigid constraint” problem in infinite honeycomb lattice is also relevant [42,53] (see also [54,55]).

### 1.1 Outline

In the following, Section 2 describes the TB model based on the nearest-neighbor hopping. Section 3 gives the details of the mathematical formulation based on Wiener–Hopf technique. Section 4 describes the exact solution of the mathematical problem. Section 5 states the asymptotic approximation of the solution deep into the two leads (left and right sides) of the junction. Section 6 presents scattering matrix for the junction and a discussion of numerical results along with expressions for the reflection and transmission coefficients. Section 7

offers the closed form expression for conductance of the junction. Discussion and conclusions appear in Section 8. Five appendices, appearing at the end of the paper, give accessory details.

## 2 Tight binding approximation and lattice model

Consider a honeycomb structure, denoted by  $\mathfrak{H}^\circ$ , containing  $N$  zigzag lines as shown in Figure 1. Indeed, from one point of view (with reference to the nanotube), the zGNR/aCNT-junction appears as a result of the removal of a zigzag semi-infinite row in an armchair nanotube. A graphical way of describing the nanotube centered perspective of the junction construction is presented in Figure 3b. Figure 3a also gives the dual perspective showing the way of describing the same structure  $\mathfrak{H}^*$  from the point of view of ribbon (with connotation that nanotubes are just rolled-up cylinders of graphene). For the purpose of problem formulation, the rectangular coordinate system, that is elaborated and introduced by [42], is used here for convenience; the same is shown schematically in Figure 4. The rectangular lattice structure  $\mathfrak{R}^\circ$ , a union of two “uncoupled” (non-interacting) honeycomb lattice ribbons  $\mathfrak{H}^\circ$  and  $\mathfrak{H}^{\circ R}$ , denoted by  $\mathfrak{R}^\circ$ , has a period  $\frac{\sqrt{3}}{2}b$  horizontally and  $\frac{3}{2}b$  vertically. A straightforward transformation<sup>2</sup> between the symbols used in [42] establishes a direct connection of the results presented there with their counterparts in the formulation of a single-orbital nearest-neighbor TB model [36] for the  $\pi$ -electron network (recall the schematic drawing in lower left side of Fig. 1) to describe the electronic states of graphene [35]. Let  $\mathbb{Z}$  denote the set of integers. Let  $\mathbb{Z}_m^n$  (for  $m \leq n$ ) denote

<sup>2</sup> See also the Section 7.3 of [50].

the set of integers  $\{m, m+1, \dots, n-1, n\}$ . With  $\beta$  representing the transfer integral between nearest-neighbor carbon sites (estimated to be about 2.75 eV in a graphene system), the well known TB Hamiltonian [35,36] for non-interacting electrons, also called Hückel Hamiltonian [56], can be written (in the second quantization) as

$$\mathcal{H} = -\beta \sum_{\mathbf{x}, \mathbf{x}^* \in 2\mathbb{Z}} \left( \sum_{\mathbf{y}, \mathbf{y}^* \in \mathbb{Z}_1^N} (a_{\mathbf{x}, \mathbf{y}}^\dagger b_{\mathbf{x}^* - 1, \mathbf{y}^*} + b_{\mathbf{x}^* + 1, \mathbf{y}^*}^\dagger a_{\mathbf{x}, \mathbf{y}}) + \sum_{\mathbf{y}, \mathbf{y}^* \in \mathbb{Z}_1^{N-1}} a_{\mathbf{x}, \mathbf{y}}^\dagger b_{\mathbf{x}^*, \mathbf{y}^*} \right) + h.c.;$$

$a_{\mathbf{x}, \mathbf{y}}^\dagger$  and  $b_{\mathbf{x}^*, \mathbf{y}^*}^\dagger$  are the *creation* operators of an electron at the  $(\mathbf{x}, \mathbf{y})$  and  $(\mathbf{x}^*, \mathbf{y}^*)$  sites in the  $(\mathbf{x}, \mathbf{y})$ th unit cell, respectively;  $a_{\mathbf{x}, \mathbf{y}}$  and  $b_{\mathbf{x}^*, \mathbf{y}^*}$  are the corresponding *annihilation* operators. Applying the quantum mechanical bra-ket notation, and the Fourier transform along  $x$ -axis, the electronic wave function is expressed as  $|\Psi(z)\rangle = \sum_{\mathbf{y}=\mathbf{y}^* \in \mathbb{Z}_1^N} (\psi_{\mathbf{y}}(z)\alpha_z^\dagger(\mathbf{y}) + \psi_{\mathbf{y}^*}(z)\beta_z^\dagger(\mathbf{y}^*))|0\rangle$ , where  $\alpha_z, \beta_z$  (resp.  $\alpha_z^\dagger, \beta_z^\dagger$ ) denote the Fourier transform of  $a_{\mathbf{x}, \cdot}, b_{\mathbf{x}, \cdot}$  (resp.  $a_{\mathbf{x}, \cdot}^\dagger, b_{\mathbf{x}, \cdot}^\dagger$ ), and  $|0\rangle$  denotes (reference) wave function in vacuum. Then, the Schrödinger equation  $\mathcal{H}(z)|\Psi(z)\rangle = \mathcal{E}(z)|\Psi(z)\rangle$ , leads to the difference equation

$$\begin{aligned} \beta^{-1} \mathcal{E} \psi_{\mathbf{y}}(z) &= -\psi_{\mathbf{y}^* - 1}(z) + \Upsilon \psi_{\mathbf{y}^*}(z), \\ \beta^{-1} \mathcal{E} \psi_{\mathbf{y}^*}(z) &= -\psi_{\mathbf{y} + 1}(z) + \Upsilon \psi_{\mathbf{y}}(z), \end{aligned} \quad (1)$$

where, for convenience of notation,  $\Upsilon$  is defined as a function of  $z$  by

$$\Upsilon(z) = -z - z^{-1}. \quad (2)$$

As shown in Figure 1, the structure  $\mathfrak{H}_\ominus^\ominus$  is composed of two parts: zigzag nanoribbon of width  $N-1$  on the left (denoted by lead B) and  $(N, N)$  armchair nanotube on the right (shown as lead A). The boundary condition for zigzag nanoribbon of width  $N-1$  is  $\psi_{\mathbf{y}^*}(z)|_{\mathbf{y}^*=0} = \psi_{\mathbf{y}}(z)|_{\mathbf{y}=N} = 0$ ; in particular, this implies that the modified equation (1) at the zigzag edges is

$$\begin{aligned} \beta^{-1} \mathcal{E} \psi_{\mathbf{y}}(z) &= \Upsilon \psi_{\mathbf{y}^*}(z), \quad \mathbf{y} = \mathbf{y}^* = 1, \\ \beta^{-1} \mathcal{E} \psi_{\mathbf{y}^*}(z) &= \Upsilon \psi_{\mathbf{y}}(z), \quad \mathbf{y} = \mathbf{y}^* = N-1, \end{aligned} \quad (3)$$

while those for the  $(N, N)$  armchair nanotube “edges” (corresponding to the periodic boundary condition, i.e., the Born-von Kármán boundary condition) are

$$\begin{aligned} \beta^{-1} \mathcal{E} \psi_{\mathbf{y}}(z) &= -\psi_{N^*}(z) + \Upsilon \psi_{\mathbf{y}^*}(z), \quad \mathbf{y} = \mathbf{y}^* = 1, \\ \beta^{-1} \mathcal{E} \psi_{\mathbf{y}^*}(z) &= -\psi_1(z) + \Upsilon \psi_{\mathbf{y}}(z), \quad \mathbf{y} = \mathbf{y}^* = N. \end{aligned} \quad (4)$$

Let  $\mathbb{Z} \times \mathbb{Z}_N$  denote the lattice coordinates of both starred and unstarred types of sites in  $\mathfrak{H}_\ominus^\ominus$ . With respect to the combined structure  $\mathfrak{H}_\ominus^\ominus$  as well as  $\mathfrak{H}_\ominus^{\ominus R}$ , let  $\Sigma$  denote

the set of all lattice sites in  $\mathfrak{X}_\ominus^\ominus$  that are assigned Dirichlet condition (corresponding to the vanishing of wave function) in the zigzag ribbon part of  $\mathfrak{H}_\ominus^\ominus$  or  $\mathfrak{H}_\ominus^{\ominus R}$ , i.e.,

$$\begin{aligned} \Sigma &= \{(\mathbf{x}, 0) \in \mathbb{Z} \times \mathbb{Z}_N : \mathbf{x} < 0\} \\ &\cup \{(\mathbf{x}^*, 0^R) \in \mathbb{Z} \times \mathbb{Z}_N : \mathbf{x}^* < 0\}. \end{aligned} \quad (5)$$

The notation  $0^R, 1^R$  has been used in (5) to emphasize the membership of the site in  $\mathfrak{H}_\ominus^{\ominus R} \subset \mathfrak{X}_\ominus^\ominus$ . The set  $\Sigma$  represents the removed zigzag half-line from the point of view of the nanotube. The same set can be also viewed as the boundary of nanoribbon (see Fig. 3 for a graphical way of describing the dual perspective). Figure 3b represents the graphical way of describing this construction, which is also adopted in the paper, as also shown in Figure 4, so that the convenient symbolism of the second problem solved by [42] can be applied as much as possible. For shorter expressions of shifted summation, sometimes in the present paper an index  $\nu$  is used in place of  $\mathbf{y}, \mathbf{y}^*$  via a mapping; see Figure 3 for a graphical explanation of the same mapping.

### 3 Wiener–Hopf formulation

#### 3.1 Incidence from nanotube

Consider an *incident electronic wave*, described by  $\psi^i, \psi^{*i}$ , with a *lattice wave vector*  $\kappa_x \in [-\pi, \pi]$ . Specifically, it is assumed that the incident lattice wave on  $\mathfrak{X}_\ominus^\ominus (= \mathfrak{H}_\ominus^\ominus \cup \mathfrak{H}_\ominus^{\ominus R})$  is given by (with  $(\mathbf{x}, \mathbf{y}), (\mathbf{x}^*, \mathbf{y}^*) \in \mathbb{Z} \times \mathbb{Z}_N$ )

$$\begin{bmatrix} \psi_{\mathbf{x}, \mathbf{y}}^i \\ \psi_{\mathbf{x}^*, \mathbf{y}^*}^{*i} \end{bmatrix} = A \begin{cases} \begin{bmatrix} a_{(\kappa^i)\nu} e^{-i\kappa_x \mathbf{x}} \\ a_{(\kappa^i)\nu}^* e^{-i\kappa_x \mathbf{x}^*} \end{bmatrix} & \text{on } \mathfrak{H}_\ominus^\ominus, \\ \begin{bmatrix} a_{(\kappa^i)N+1-\nu}^* e^{-i\kappa_x \mathbf{x}^*} \\ a_{(\kappa^i)N+1-\nu} e^{-i\kappa_x \mathbf{x}} \end{bmatrix} & \text{on } \mathfrak{H}_\ominus^{\ominus R}, \end{cases} \quad (6)$$

where  $A \in \mathbb{C}$  is constant. The notation  $a_{(\kappa^i)\cdot}$  and  $a_{(\kappa^i)\cdot}^*$  stands for the modeshape [50] of  $\kappa^i$ th wave mode in *armchair nanotube*  $\mathfrak{H}_\ominus^\ominus$ . As a major step towards simplification of the problem, following [42], the even reflection symmetry on  $\mathfrak{X}_\ominus^\ominus$  has been “manufactured” through the peculiar choice of the incident wave ansatz (6). In this context, the manufactured even reflection symmetry should not be confused with the intrinsic even or odd symmetry, in other words, the even and odd reflection symmetry of a mode on  $\mathfrak{H}_\ominus^\ominus$  (either of the two terminals) uses (for coordinates) a rectangular lattice strip  $\mathfrak{X}_\ominus^\ominus$  which is distinct from the assumed structure  $\mathfrak{H}_\ominus^\ominus$  or  $\mathfrak{H}_\ominus^{\ominus R}$  (see also Appendix B.4). In equivalent terms, the “manufactured” even reflection symmetry on  $\mathfrak{X}_\ominus^\ominus$  is simply the construction of a symmetric incident wave in terms of any arbitrary<sup>3</sup> wave mode on the armchair nanotube<sup>4</sup>  $\mathfrak{H}_\ominus^\ominus$  [50], i.e.,  $\mathbb{1}_{a_{(\kappa^i)\mathbf{y}}} = a_{(\kappa^i)-\mathbf{y}^*}^*$ ,

<sup>3</sup> Implying there is no loss of generality by imposing such reflection symmetry; in general, the reflection symmetry *does not* hold on either side of the junction for  $(N, N)$ -aCNT  $\mathfrak{H}_\ominus^\ominus$  or  $(N-1)$ -zGNR  $\mathfrak{H}_\ominus^{\ominus R}$ .

<sup>4</sup> By virtue of single rolling  $N = 2N$ , i.e., it is an even number.

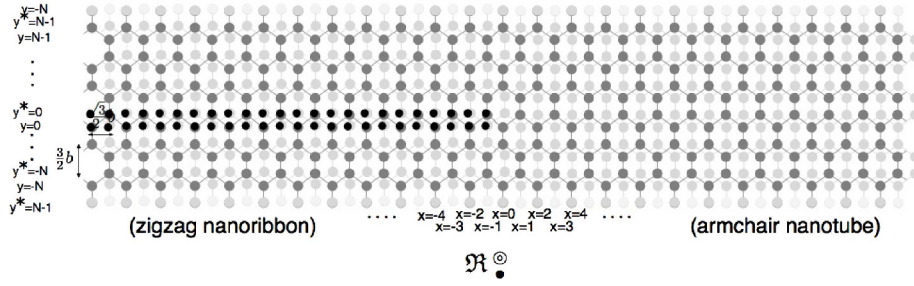


**Fig. 4.** Illustration of the rectangular coordinates [42,53] for the honeycomb lattice structure  $\mathfrak{H}_{\pm}^{\circledast}$ . Here  $\mathfrak{R}_{\pm}^{\circledast} = \mathfrak{H}_{\pm}^{\circledast} \cup \mathfrak{H}_{\pm}^{\circledast R}$ .

$y = y^* \in \mathbb{Z}_0^{N-1}$ , where the symbol  $\mathfrak{J}$  equals  $+$  for even mode and  $-$  for odd mode. For convenience of mathematical manipulations, the total wave function  $\psi^t$  at the lattice sites is split into a scattered part  $\psi^s$  and the incident wave mode  $\psi^i$ , i.e.,

$$\psi_{x,y}^t = \psi_{x,y}^i + \psi_{x,y}^s, \psi_{x^*,y^*}^{*t} = \psi_{x^*,y^*}^{*i} + \psi_{x^*,y^*}^{*s}. \quad (7)$$

In order to ensure causality, a vanishingly small amount of absorption is assumed [57] so that  $\mathcal{E} \simeq \mathcal{E} + i0$ . The discrete Helmholtz equation (corresponding to (1)) on the honeycomb lattice structure  $\mathfrak{H}_{\pm}^{\circledast}$  is

$$\psi_{x^*+1,y^*}^{*t} + \psi_{x^*-1,y^*}^{*t} + \psi_{x^*,y^*-1}^{*t} + \beta^{-1}\mathcal{E}\psi_{x^*,y^*}^t = 0, \quad (8a)$$

$$\psi_{x+1,y}^t + \psi_{x-1,y}^t + \psi_{x,y+1}^t + \beta^{-1}\mathcal{E}\psi_{x,y}^{*t} = 0, \quad (8b)$$

for  $(x, y) \in \mathbb{Z} \times \mathbb{Z}_N \setminus \Sigma$ , and  $(x^*, y^*) \in \mathbb{Z} \times \mathbb{Z}_N \setminus \Sigma$ , respectively (recall that  $\Sigma$  is given by (5)). With  $\psi^t = \psi^i, \psi^{*t} = \psi^{*i}$  (given by (6)), the incident wave mode index  $\kappa^i$  and incident wave number  $\kappa_x$  must satisfy the appropriate energy band relation condition [50] for the given energy  $\mathcal{E}$  according to (8). The expressions for the wavemode components in (6) naturally depend on the choice of these incident wave parameters [50]. From the point of view of scattering theory [41], the incident wave, described by  $\psi^i$  and  $\psi^{*i}$  (6), on  $\mathfrak{R}_{\pm}^{\circledast}$  interacts with a slit on negative  $x$ -axis of the nanotube (see Fig. 3b). Following the notation and definitions similar to that for the discrete Sommerfeld problems on the infinite honeycomb lattice [42], using the Fourier transform  $\psi_y^F$  and  $\psi_{y^*}^{*F}$  (A.1) of the functions  $\psi_y$  and  $\psi_{y^*}^*$ , respectively, the equation (8) is expressed as (same as (1))

$$\begin{aligned} \beta^{-1}\mathcal{E}\psi_y^F &= \Upsilon\psi_{y^*}^{*F} - \psi_{y^*-1}^{*F}, \\ \beta^{-1}\mathcal{E}\psi_{y^*}^{*F} &= \Upsilon\psi_y^F - \psi_{y+1}^F, \end{aligned} \quad (9)$$

for all  $y \in \mathbb{Z} \setminus \{0\}, y^* \in \mathbb{Z} \setminus \{-1\}$ . As mentioned above (Footnote 4), the periodic boundary conditions are possible (by rolling a zigzag ribbon) only when  $N$  is an even number. The general solution (A.7) using the periodic condition can be constructed as described in Appendix A.

Finally, the boundary conditions in the problem, i.e., vanishing of the wave function, associated with  $\Sigma$  (5) need to be tackled. In fact,  $\psi_{x+1,0} + \psi_{x-1,0} + \psi_{x,1} + \beta^{-1}\mathcal{E}\psi_{x,0} = 0, x \geq 0$ , using the even reflection symmetry on  $\mathfrak{R}_{\pm}^{\circledast}$  by

virtue of the chosen form of incident wave  $\psi^i$  (6) on the union of sub-lattice  $\mathfrak{H}_{\pm}^{\circledast}$  and the “replicated” sub-lattice  $\mathfrak{H}_{\pm}^{\circledast R}$ ; also by the same reasoning the scattered wave function satisfies  $\psi_0^F = \psi_{0^*}^{*F}$  and  $\psi_{1,+}^F = \psi_{-1,+}^{*F}, \psi_{1,-} = \psi_{-1,-}^*$ . The introduction of rectangular coordinates, and the manufactured symmetry, facilitates the application of discrete analysis developed in a recent series of papers [42,58]. Applying the discrete Fourier transform on equation (8) for  $y = 0, x \geq 0$ , and (5), respectively, it follows that

$$\mathcal{P}(z)\psi_{0,+}(z) = \mathcal{W}(z) + \psi_{1,+}(z), \quad z \in \mathcal{A}, \quad (10a)$$

$$\psi_{0,-}(z) = -A\mathfrak{J}a^i\delta_{D-}(\mathfrak{J}zz_P^{-1}), \quad z \in \mathcal{C}, |z| < R_-, \quad (10b)$$

$$\text{where } \mathcal{W}(z) := -z\psi_{0,0} + \psi_{-1,0}, \quad z \in \mathcal{C}, \quad (10c)$$

$$\mathcal{P} := -\beta^{-1}\mathcal{E} + \Upsilon, \quad (10d)$$

and  $z_P, \delta_{D-}$  are defined by

$$z_P := e^{-i\kappa_x} \in \mathbb{C}, \quad (11)$$

$$\text{and } \delta_{D-}(z) := \sum_{n=-\infty}^{-1} z^{-n}, \quad z \in \mathbb{C} \text{ such that } |z| < 1. \quad (12)$$

Notice that  $|z_P| > 1$  when  $\Im \mathcal{E} > 0$ . For incidence from the nanotube side of  $\mathfrak{H}_{\pm}^{\circledast}$  as discussed in this section, the scalar  $a^i$  appearing in (10b) is defined by (see Appendix B.4)

$$a^i := \mathfrak{J}a^{(\kappa^i)}_{\nu}|_{y=0} = a^{*(\kappa^i)}_{\nu}|_{y^*=0} = a^{*(\kappa^i)}_1, \quad (13)$$

using the relation, between the indices  $\nu$  and the vertical coordinate  $y, y^*$  for the armchair nanotube rows, on the right according to the symmetric modes [50]; see Figure 3b for the  $\nu-y, y^*$  relation. In (10a), the domain  $\mathcal{A}$  is an annulus in the complex plane, which is defined by (C.7) in Appendix C. From (9) for  $y = 1$ , after some calculations involving the definition of  $\lambda$  (as detailed in Appendix A), the discrete Wiener–Hopf equation is obtained as

$$\mathcal{L}\psi_{1,+} + \psi_{1,-} = (1 - \mathcal{L})(\mathcal{W} + \mathcal{P}\psi_{0,-}) \text{ on } \mathcal{A}, \quad (14a)$$

$$\text{where } \mathcal{L} := 1 - \frac{\mathcal{M}_N}{\mathcal{P}}, \quad (14b)$$

and  $\mathcal{M}_N$  is defined by

$$\mathcal{M}_N = \frac{\mathcal{P}U_{N-2} - U_{N-1}}{U_{N-2} - \mathcal{P}U_{N-1}}, \quad (15)$$

with the argument of the Chebyshev polynomials  $U_n (= U_n(\vartheta))$ ,  $\vartheta$  [46,47], defined by

$$\vartheta = \frac{1}{2} \left( -\frac{(\beta^{-1}\mathcal{E} - 1)(\beta^{-1}\mathcal{E} + 1)}{\Upsilon} + \Upsilon \right). \quad (16)$$

Recall that  $\Upsilon$  is defined by (2). By the definition of  $Q$  (A.3), it is easy to see that  $(\beta^{-1}\mathcal{E})^2 = \Upsilon^2 + 1 - \Upsilon Q$ , and  $\vartheta = \frac{1}{2} Q$ . The Wiener–Hopf kernel (14b) is further rewritten, in terms of the Chebyshev polynomials of the second kind, as

$$\mathcal{L} = \frac{1}{\mathcal{P}} \frac{(1 - \mathcal{P}^2) U_{N-1}}{U_{N-2} - \mathcal{P} U_{N-1}} = \frac{\mathcal{N}}{\mathcal{D}} = \frac{\mathcal{N}}{\mathcal{P} \widehat{\mathcal{D}}}. \quad (17)$$

In the above form (17), in view of the recent expressions provided by [50], it is seen that the denominator of  $\mathcal{L}$ , i.e.,  $U_{N-2} - \mathcal{P} U_{N-1}$ , represents the energy bands for the even symmetric modes on the rectangular lattice structure  $(\mathfrak{H}_{\bullet\bullet}^* \cup \mathfrak{H}_{\bullet\bullet}^{*\text{R}})$  containing the zigzag nanoribbon  $\mathfrak{H}_{\bullet\bullet}^*$  of width  $N - 1$ , while the numerator  $(1 - \mathcal{P}^2) U_{N-1}$  represents the energy bands for the even symmetric modes on the rectangular lattice structure  $(\mathfrak{H}_{\circ} \cup \mathfrak{H}_{\circ}^{\text{R}})$  containing the armchair nanotube  $\mathfrak{H}_{\circ}$  (of width  $N$ ). In this context, recall Footnote 3 also. See also Appendix B for the details concerning the energy bands and symmetric wave modes based on the relevant portions from [50].

### 3.2 Incidence from nanoribbon

It is assumed that the incident wave,  $\psi^i$  and  $\psi^{*i}$ , is described by the same expression (6) on  $\mathfrak{X}_{\ominus}^{\oplus}$  as above, however, the modeshape  $a_{(\kappa^i)}$  and  $a_{(\kappa^i)}^*$  pertains to the  $\kappa^i$ th wave mode in the zigzag nanoribbon  $\mathfrak{H}_{\bullet\bullet}^*$  [50]. Again, it is noteworthy for the terminal  $\mathfrak{H}_{\bullet\bullet}^*$  that  $\mathfrak{I} a_{(\kappa^i)\mathbf{y}} = a_{(\kappa^i) - \mathbf{y}^*}$ ,  $\mathbf{y} = \mathbf{y}^* \in \mathbb{Z}_0^{N-1}$ , where it is to be recalled that the parity bit  $\mathfrak{I}$  is + for even mode and – for odd mode. From the point of view of scattering theory [41], the incident wave encounters the additional hopping interactions on the two zigzag boundaries along the positive  $x$ -axis of the nanoribbon (see Fig. 3a). Recall the (manufactured) even reflection symmetry and the boundary conditions on the ribbon side of  $\mathfrak{X}_{\ominus}^{\oplus}$ ,<sup>5</sup> in particular, the equation  $\psi_{0-} = \psi_{0-}^* = 0$  holds. After applying the discrete Fourier transform to equation (8) for  $\mathbf{y} = 0, \mathbf{x} \geq 0$ , i.e.,  $\psi_{\mathbf{x}+1,0} + \psi_{\mathbf{x}-1,0} + \psi_{\mathbf{x},1} + \psi_{\mathbf{x},1}^i + \beta^{-1}\mathcal{E}\psi_{\mathbf{x},0} = 0, \mathbf{x} \geq 0$ , and that corresponding to (5), respectively, it follows that (on the lines of the recently published general manipulations [42,58])

$$\mathcal{P}(z)\psi_{0,+}(z) = \mathcal{W}(z) + \psi_{1,+}^i(z) + \psi_{1,+}(z), \quad z \in \mathcal{A}, \quad (18a)$$

$$\psi_{1,+}^i(z) = \mathfrak{A} \mathfrak{I} a_{(\kappa^i)} \delta_{D+}(\mathfrak{I} z z_{\mathcal{P}}^{-1}), \quad z \in \mathbb{C}, |z| < R_-, \quad (18b)$$

<sup>5</sup> The incident wave  $\psi^i, \psi^{*i}$  (6), on sub-lattices  $\mathfrak{H}_{\ominus}^{\oplus}$  and “replicated” sub-lattice  $\mathfrak{H}_{\ominus}^{\oplus\text{R}}$ , is “even” (note that the zigzag nanoribbon has odd width  $N - 1 = 2N - 1$ ) [50], i.e.,  $a_{(\kappa^i)\mathbf{y}} = a_{(\kappa^i)N - \mathbf{y}^*}$ ,  $\mathbf{y} = \mathbf{y}^* \in \mathbb{Z}_0^N$ ; observe that by construction of even reflection symmetry and vanishing wave function the boundary condition  $a_{(\kappa^i)0} = a_{(\kappa^i)N} = 0$ .

where

$$\delta_{D+}(z) := \sum_{n=0}^{+\infty} z^{-n}, \quad z \in \mathbb{C} \text{ such that } |z| > 1, \quad (19)$$

$\mathcal{W}$  is given by (10c), while  $z_{\mathcal{P}}$  is defined by (12). Notice that  $|z_{\mathcal{P}}| < 1$  whenever  $\Im \mathcal{E} > 0$ . As in the previous case of incidence,  $\mathcal{A}$  is an annulus in the complex plane, which is defined by (C.7). For present case of incidence from the nanoribbon side of  $\mathfrak{H}_{\ominus}^{\oplus}$ , the scalar  $a^i$  in (18b) is defined by (see Appendix B.4)

$$a^i := \mathfrak{I} a_{(\kappa^i)\nu}|_{\mathbf{y}=1} = a_{(\kappa^i)\nu}|_{\mathbf{y}^*=-1} = a_{(\kappa^i)N}, \quad (20)$$

using the mapping of indices  $\nu$  and coordinate  $\mathbf{y}, \mathbf{y}^*$  for the zigzag nanoribbon rows on the left according to the symmetric modes [50]; see Figure 3a for the relation between  $\nu$  and  $\mathbf{y}, \mathbf{y}^*$ . Using (15), the discrete Wiener–Hopf equation is obtained as

$$\mathcal{L}\psi_{1,+} + \psi_{1,-} = (1 - \mathcal{L})(\mathcal{W} + \psi_{1,+}^i) \text{ on } \mathcal{A}, \quad (21)$$

where  $\mathcal{L}$  is same as that given by (14b) (and the simplified form (17)). It is interesting to note the contrast between the right side of (21) and that of (14a) as well as between (20) and (13).

## 4 Exact solution

Suppose that, as an implicit notation, which is used throughout the rest of the paper, the symbol  $\mathfrak{s}$  denotes any of the two cases of the incidence, i.e.,  $\mathfrak{s} = \text{A}$  represents the incidence from the right (nanotube-side) while  $\mathfrak{s} = \text{B}$  represents the incidence from the left (nanoribbon-side) with respect to the schematic shown in Figure 1. Consider the case of even reflection symmetry, i.e., when the parity bit  $\mathfrak{I}$  is +. A standard procedure [41], as also described in Appendix C, provides the solution of the discrete Wiener–Hopf equations (14a) and (21) as

$$\begin{aligned} \psi_{1,+}(z) &= \frac{C_+(z)}{\mathcal{L}_+(z)}, \\ \psi_{1,-}(z) &= C_-(z)\mathcal{L}_-(z), \quad z \in \mathcal{A}, \end{aligned} \quad (22)$$

where  $\mathcal{L}_{\pm}, C_{\pm}$  are given by (C.6) and (C.10). Using (22) in (10a), the expression for  $\psi_{0,+}$ , in terms of  $\psi_{0,0}$ , can be determined, which leads to the solution of the wave propagation problem in the form of a discrete Fourier transform, albeit with striking presence of the undetermined scalar  $\psi_{0,0}$ . By an application of the inverse discrete Fourier transform

$$\psi_{\mathbf{x},\mathbf{y}} = \frac{1}{2\pi i} \oint_{\mathbb{T}} \psi_{\mathbf{y}}^F(z) z^{\mathbf{x}-1} dz, \quad (23)$$

on  $\psi_0^F$ , and some intermediate calculations, using the Cauchy residue theorem [59],  $\psi_{0,0}$  is obtained and simplifying the resulting expression, it is found that

$$\begin{aligned} \psi_{0,0}^t &= -Aa^i \frac{\mathcal{L}_+(z_P)\mathcal{P}(z_P)}{l_{+0}(z_P - z_P^{-1})} \delta_{s,A} \\ &+ \frac{Aa^i}{\mathcal{P}(z_P)} \frac{\mathcal{L}_-^{-1}(z_P)(1 - z_P z_P^{-1})}{l_{+0}} \delta_{s,B}. \end{aligned} \quad (24)$$

Finally, the complete solution of the electronic wave transmission problem, in the form of a discrete Fourier transform is given by

$$\psi_0^F(z) = A \frac{C_0}{z - z_P} z \mathcal{K}(z), \quad z \in \mathcal{A}, \quad (25)$$

$$\begin{aligned} \text{where } C_0 &:= a^i \frac{\mathcal{L}_+(z_P)\mathcal{P}(z_P)}{z_P^{-1} - z_P} \delta_{s,A} \\ &+ a^i \frac{\mathcal{L}_-^{-1}(z_P)}{\mathcal{P}(z_P)} (1 - z_P z_P^{-1}) \delta_{s,B} \in \mathbb{C}, \end{aligned} \quad (26)$$

$$\text{and } \mathcal{K}(z) := \frac{1}{(1 - z_P z^{-1})\mathcal{L}_+(z)}, \quad z \in \mathcal{A}. \quad (27)$$

Recall that  $a^i$  is given by (13) and (20) for  $s = A$  and  $s = B$ , respectively. In the same context, note that  $\mathfrak{J}$  is allowed to be  $+$  or  $-$  for both directions of incidence. But it is a matter of great relief that above analysis can be easily repeated for the case of odd reflection symmetry of the incident electronic wave mode, i.e., when  $\mathfrak{J}$  is  $-$ . In fact, it is found that the only change in the expressions (25) and (26) is that  $z_P$  is replaced by  $-z_P$ . The expression (25) is the key to provide the exact solution of the electronic wave transmission problem in all zigzag lines, as the electronic wave function in the rectangular lattice structure is given by (A.7a) using (25) and the (manufactured) even reflection symmetry (A.7b) on  $\mathfrak{R}^\ominus$ . In the context of the results of [42], by virtue of the symmetry of incident wave mode on  $\mathfrak{R}^\ominus$ , only one term out of the two terms stated in (6.18)–(6.21) by [42] contributes to the exact solution (25). In fact, without the assumption of the symmetry in the incident wave mode (hidden in the parity  $\mathfrak{J}$ ), both terms appear.

The exact solution, on the rectangular structure, as stated above can be dissected further to yield the expression on the honeycomb structure. Indeed, by (23) and (25), on the physical lattice structure (as  $\mathbf{x} \in 2\mathbb{Z} + 1$  for  $y = 1$  and  $\mathbf{x}^* \in 2\mathbb{Z}$  for  $y^* = -1$ , for example, see Fig. 4),

$$\begin{aligned} \psi_{x,1} &= \frac{1}{2\pi i} \oint_{\mathbb{T}} \frac{1}{2} (\psi_1^F(z) - \psi_1^F(-z)) z^{\mathbf{x}-1} dz, \\ \psi_{x^*,-1}^* &= \frac{1}{2\pi i} \oint_{\mathbb{T}} \frac{1}{2} (\psi_{-1}^{*F}(z) + \psi_{-1}^{*F}(-z)) z^{\mathbf{x}^*-1} dz. \end{aligned} \quad (28)$$

## 5 Asymptotic approximation

Using the mode-matching method [51,60], the wave function deep inside the leads (the two portions, namely the

zigzag nanoribbon  $\mathfrak{N}^{\bullet*}$  and the armchair nanotube  $\mathfrak{N}^\circ$ ), as schematically shown in Figure 5, can be determined solely in terms of the eigenmodes [50] associated with them. Note that the concerned analysis of [50] yields expressions, which have been found earlier as well (for instance, see [61]); the choice of coordinates needs to be carefully mapped though, for example Appendix D provides a mapping between the rectangular coordinates (employed in the present paper following [42,53]) and slant coordinates. The determination of the coefficients in such an eigenmodes expansion can be done in an exact manner for this problem using the completeness of the eigenmodes (propagating waves for a given energy level  $\mathcal{E}$ ); the same is a highlight of the present paper. A comparison of the wave function  $\psi_{x,1}$  (see also (28)) determined by (22) and (23) (as well as the residue calculus for contour integrals, see [62] for the relevant mathematical analysis in case of square lattice waveguides) with its counterpart obtained by the eigenmode expansion in the two leads (as shown in Fig. 5) results in the determination of these coefficients. The accompanying residues are evaluated at  $z$ , which expectedly correspond to the outgoing waves ahead and behind the zGNR/aCNT-junction; the same are, respectively, (with even reflection symmetry)

$$\begin{aligned} \mathcal{Z}_{eA}^+ &= \{z \in \mathbb{T} \mid \mathcal{N}_+(z) = 0\}, \\ \mathcal{Z}_{eB}^- &= \{z \in \mathbb{T} \mid \widehat{\mathcal{D}}_-(z) = 0\}, \end{aligned} \quad (29)$$

and (with odd reflection symmetry)

$$\begin{aligned} \mathcal{Z}_{oA}^+ &= \{z \in \mathbb{T} \mid \mathcal{N}_+(-z) = 0\}, \\ \mathcal{Z}_{oB}^- &= \{z \in \mathbb{T} \mid \widehat{\mathcal{D}}_-(-z) = 0\}. \end{aligned} \quad (30)$$

Analogous to (17), based on the discussion in Appendix B.4, consider the definitions

$$\mathcal{N}_o(z) := \mathcal{N}(-z), \widehat{\mathcal{D}}_o(z) := \widehat{\mathcal{D}}(-z). \quad (31)$$

Eventually, it is found that the total wavefunction for the incidence from the right ( $s = A$ ), recall Section 3.1, is given by (an analogue corresponding to the starred sites is stated by placing  $a^*_{\pm(\kappa)\nu}$  in stead of  $a_{\pm(\kappa)\nu}$ )

$$\begin{aligned} \psi_{x,y}^t &\sim Aa_{(\kappa^i)\nu} z_P^{\mathbf{x}} \\ &+ \frac{1}{2} A \frac{\mathcal{N}_+(z_P)}{\widehat{\mathcal{D}}_+(z_P)} \left( \sum_{z \in \mathcal{Z}_{eA}^+} \frac{a^i}{a^*_{+(\kappa_z)1}} \frac{\widehat{\mathcal{D}}_+(z)}{\mathcal{N}'_+(z)} \frac{a_{+(\kappa_z)\nu} z^{\mathbf{x}}}{z - z_P} \right. \\ &\quad \left. - \sum_{z \in \mathcal{Z}_{oA}^+} \frac{a^i}{a^*_{+(\kappa_z)1}} \frac{\widehat{\mathcal{D}}_{o+}(z)}{\mathcal{N}'_{o+}(z)} \frac{a_{+(\kappa_z)\nu} z^{\mathbf{x}}}{z + z_P} \right), \\ \psi_{x,y}^t &\sim \frac{1}{2} A \frac{\mathcal{N}_+(z_P)}{\widehat{\mathcal{D}}_+(z_P)} \left( \sum_{z \in \mathcal{Z}_{eB}^-} \frac{a^i}{a^*_{-(\kappa_z)N}} \frac{\mathcal{N}_-(z)}{\widehat{\mathcal{D}}'_-(z)} \frac{a_{-(\kappa_z)\nu} z^{\mathbf{x}}}{z - z_P} \right. \\ &\quad \left. - \sum_{z \in \mathcal{Z}_{oB}^-} \frac{a^i}{a^*_{-(\kappa_z)N}} \frac{\mathcal{N}_{o-}(z)}{\widehat{\mathcal{D}}'_{o-}(z)} \frac{a_{-(\kappa_z)\nu} z^{\mathbf{x}}}{z + z_P} \right), \end{aligned} \quad (32)$$

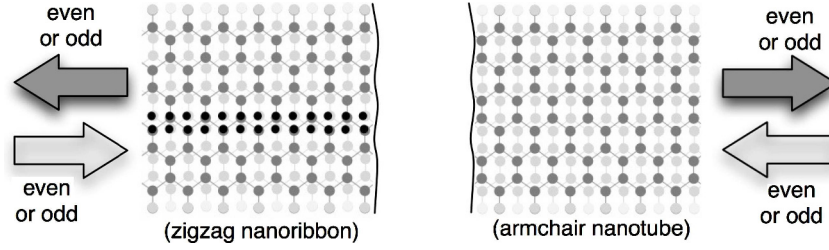


**Fig. 5.** Schematic construction of the incident electronic wave mode in lead B and lead A.

as  $x \rightarrow +\infty$  and  $x \rightarrow -\infty$ , respectively. In (32), the notation  $\kappa_z$  indicates that  $\kappa_z$ th mode is used for given  $z$  corresponding to the summand; also the notation  $a_{+(\kappa_z)}$  (resp.  $a_{-(\kappa_z)}$ ) represents the  $\kappa_z$ th modeshape for the lead on the right (resp. left). Analogously, the total wavefunction for the incidence from the left ( $\mathfrak{s} = B$ ), recall Section 3.2, is given by (again, the analogous expression corresponding to the starred sites is easy to state by using  $a^*_{\pm(\kappa)\nu}$  in place of  $a_{\pm(\kappa)\nu}$ )

$$\begin{aligned} \psi_{x,y}^t &\sim A \frac{\widehat{D}_-(z_P)}{N_-(z_P)} \frac{1}{2} \left( \sum_{z \in \mathcal{Z}_{eA}^+} \frac{a^i}{a^*_{+(\kappa_z)1}} \frac{\widehat{D}_+(z)}{N'_+(z)} \frac{a_{+(\kappa_z)\nu} z^x}{z - z_P} \right. \\ &\quad \left. - \sum_{z \in \mathcal{Z}_{oA}^+} \frac{a^i}{a^*_{+(\kappa_z)1}} \frac{\widehat{D}_{o+}(z)}{N'_{o+}(z)} \frac{a_{+(\kappa_z)\nu} z^x}{z + z_P} \right), \\ \psi_{x,y}^t &\sim A a_{(\kappa^i)\nu} z_P^x + A \frac{\widehat{D}_-(z_P)}{N_-(z_P)} \\ &\quad \times \frac{1}{2} \left( \sum_{z \in \mathcal{Z}_{eB}^-} \frac{a^i}{a^*_{-(\kappa_z)N}} \frac{N_-(z)}{\widehat{D}'_-(z)} \frac{a_{-(\kappa_z)\nu} z^x}{z - z_P} \right. \\ &\quad \left. - \sum_{z \in \mathcal{Z}_{oB}^-} \frac{a^i}{a^*_{-(\kappa_z)N}} \frac{N_{o-}(z)}{\widehat{D}'_{o-}(z)} \frac{a_{-(\kappa_z)\nu} z^x}{z + z_P} \right), \end{aligned} \quad (33)$$

as  $x \rightarrow +\infty$  and  $x \rightarrow -\infty$ , respectively.

Complementary to the set of  $z$  corresponding to outgoing waves (with even symmetry) (29), those corresponding (with even symmetry) to incoming waves (i.e., travelling towards the junction so that  $z_P = z \in \mathcal{Z}_{eA}^-$  for  $\mathfrak{s} = A$ , as discussed in Sect. 3.1, while  $z_P = z \in \mathcal{Z}_{eB}^+$  for  $\mathfrak{s} = B$ , as discussed in Sect. 3.2) are

$$\begin{aligned} \mathcal{Z}_{eA}^- &= \{z \in \mathbb{T} \mid N_-(z) = 0\}, \\ \mathcal{Z}_{eB}^+ &= \{z \in \mathbb{T} \mid \widehat{D}_+(z) = 0\}. \end{aligned} \quad (34)$$

Similarly, the incoming waves with odd reflection symmetry are given by (see also Appendix B.4)

$$\begin{aligned} \mathcal{Z}_{oA}^- &= \{z \in \mathbb{T} \mid N_-(-z) = 0\}, \\ \mathcal{Z}_{oB}^+ &= \{z \in \mathbb{T} \mid \widehat{D}_+(-z) = 0\}. \end{aligned} \quad (35)$$

Let

$$\begin{aligned} \mathcal{Z}_A^+ &= \mathcal{Z}_{eA}^+ \cup \mathcal{Z}_{oA}^+, \\ \mathcal{Z}_B^- &= \mathcal{Z}_{eB}^- \cup \mathcal{Z}_{oB}^-, \\ \tilde{\mathcal{Z}}_A^+ &= \tilde{\mathcal{Z}}_{eA}^+ \cup \tilde{\mathcal{Z}}_{oA}^+, \\ \tilde{\mathcal{Z}}_B^- &= \tilde{\mathcal{Z}}_{eB}^- \cup \tilde{\mathcal{Z}}_{oB}^-. \end{aligned} \quad (36)$$

Note that  $\#\mathcal{Z}_{eA}^\pm = \#\mathcal{Z}_{oA}^\pm$ ,  $\#\mathcal{Z}_{eB}^\pm = \#\mathcal{Z}_{oB}^\pm$ ,  $\#\mathcal{Z}_A^+ = \#\tilde{\mathcal{Z}}_A^-$ ,  $\#\mathcal{Z}_B^+ = \#\tilde{\mathcal{Z}}_B^-$  and that  $z_P \in \mathcal{Z}_A^-$  for the incidence from nanotube while  $z_P \in \tilde{\mathcal{Z}}_B^+$  for the incidence from nanotube. For  $z_P \in \mathcal{Z}_{oA}^+$  and  $z_P \in \mathcal{Z}_{oB}^+$ , respectively, the expressions (32) and (33) are modified with the replacement of  $z_P$  by  $-z_P$ .

An illustration of the numerical solution of the discrete Helmholtz problem, based on the scheme summarized in Appendix D (essentially same as that stated by [42] modulo the removal of upper and lower absorbing layers, i.e., including only the left and right absorbing layers), is provided in part (a) of Figures 6–11 for a given energy level  $\mathcal{E}$  (in terms of the transfer integral  $\beta$ ) and incident wave number  $\kappa_x$ . The contour plots of the real part of the total wave function  $\Re\psi^t$ ,  $\Re\psi^{*t}$  as well as the modulus of the scattered wave function  $|\psi|$ ,  $|\psi^*|$  are shown on the honeycomb structure  $\mathfrak{H}_\pm^\ominus$  (and *not*  $\mathfrak{H}_\pm^{\ominus R}$  or  $\mathfrak{R}_\pm^\ominus$ ). The symbols  $N_{\text{grid}}$ ,  $N_{\text{pml}}$  are described in Appendix D. The propagating wave modes (with  $z = e^{-i\xi}$  in relation to the definitions (29)), which contribute to the far-field in the reflected and transmitted wave function, are also shown in the corresponding part (b) for the chosen energy value  $\mathcal{E}$  (in terms of the transfer integral  $\beta$ ). The parts (c), (d), and (e) present the validated results showing agreement between the numerical solution and the asymptotic approximation of the exact solution on a rectangular shaped set of sites shown in part (a) as white square bubbles. By an observation of the fine agreement between the numerical solution and the asymptotic approximation, it is concluded that the far field wavefunction is dominated (almost equals) by its approximation in terms of wave modes in the pass band allowed by the energy bands of the respective portion on the left and right side of junction. Figures 6, 8, and 10 provide the results for the incidence from the tubular side (formulated in Sect. 3.1), whereas Figures 7, 9, and 11 provide the results for the incidence from the ribbon side (formulated in Sect. 3.2). Figures 6 and 7 provide the results for energy much below the Fermi level (i.e., away

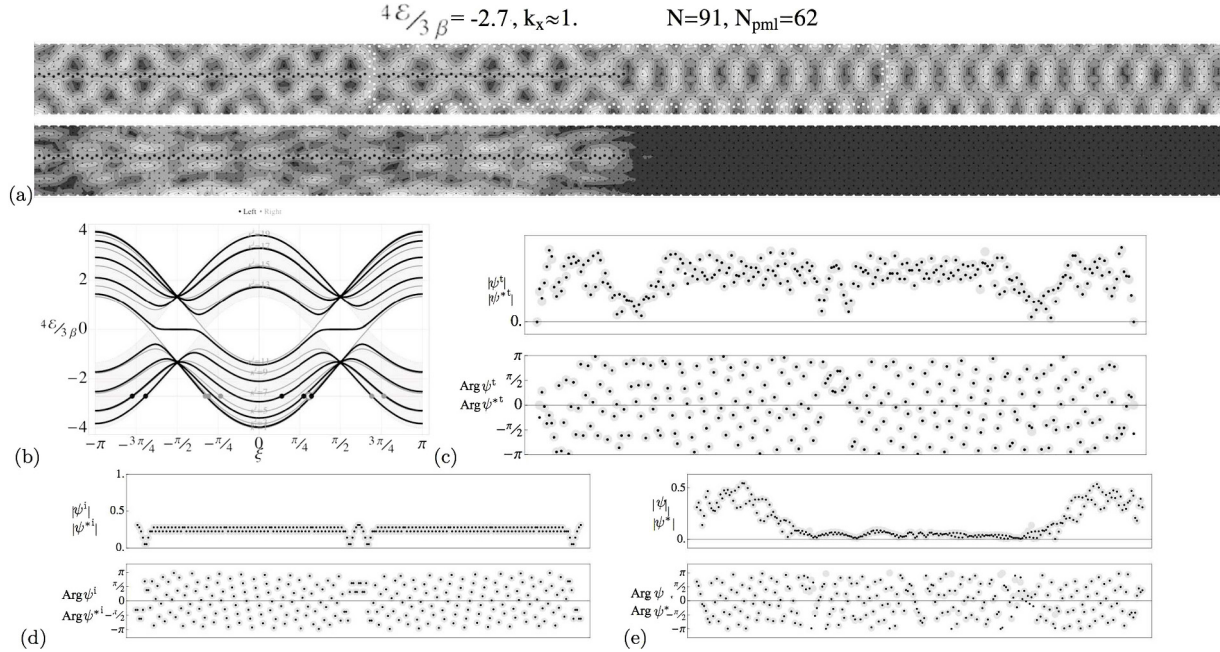


**Fig. 6.** Plots for the case of incidence of an even mode from nanotube side of the wave-guide. (a) The contour plot of  $\Re\psi^t, \Re\psi^{*t}$ , is shown in the top portion, while  $|\psi|, |\psi^*|$ , is shown on the bottom. The small black dots show the honeycomb structure. The big black dots represent the sites where wave function vanishes and white dots correspond to the glued part due to “periodic” condition. (b) Energy bands for the wave modes ahead, with symmetry, and behind the junction. The red dots represent the wave numbers reflected by the defect tip while green dots represent those transmitted in front of the defect (gray dot represents the incident wave number). Comparison of (c)  $|\psi^i|, \arg \psi^i$ , (d)  $|\psi|, \arg \psi$ , (e)  $|\psi^t|, \arg \psi^t$  between the closed form expression using normal modes based far-field approximation and the numerical solution on a finite grid. The horizontal axis corresponds to the integral labels for the lattice sites forming discrete rectangles of white square bubbles shown in part (a). In all plots  $N = 10$ .

from the Dirac points [63]) but incident wavenumber less than  $\pi/2$  in magnitude, while Figures 8 and 9 provide the results for almost the same energy level but with incident wavenumber more than  $\pi/2$  in magnitude. In contrast, Figures 10 and 11 provide the results for the energy close to the well known Fermi level (occurring close to the Dirac points) for graphene-like structures [4]. The structure of the energy band in the middle of part (b) of the plots shown, which is a descendant of the “flat” band [8,64] in the presence of confinement, depends on the details [63] of the electronic model (one of the major effects being the electron–electron interaction [27]) and hopping interactions [65]; the investigation of the same with respect to relevant perturbations [66,67] lies outside the scope of present paper.

### 6 Scattering matrix

Suppose that the elements of  $\mathcal{L}_A^+$  (resp.  $\tilde{\mathcal{L}}_A^-$ ) are indexed<sup>6</sup> by  $a$  (resp.  $\tilde{a}$ ) with a range  $1 \dots N^A = \#\mathcal{L}_A^+$ , while the elements of  $\mathcal{L}_B^-$  (resp.  $\tilde{\mathcal{L}}_B^+$ ) are indexed by  $b$  (resp.  $\tilde{b}$ ) ranging from 1 to  $N^B = \#\mathcal{L}_B^-$ . Henceforth in the context

<sup>6</sup>For the purpose of the ordering, one possible and easy choice is to associate the index with the energy bands for different modes in the either side of the junction, labelled according to increasing values of  $\mathcal{E}$  at  $\xi = 0$ .

of the expressions such as (32) and (33), the superscript  $t$  on the total wave function  $\psi, \psi^*$  is ignored.

For the incidence from the nanotube, ahead and behind the junction, respectively, assuming  $z_P$  corresponds to the index  $\tilde{a}$  in (32), i.e.,  $z_P = z_{\tilde{a}}$ , the inspection of (32) reveals that

$$\begin{aligned} \psi_{x,y} &\sim A a_{(\tilde{a})y} z_{\tilde{a}}^x + A \sum_{a=1}^{N^A} \mathcal{J}_{\tilde{a}a}^{\tilde{A}A} a_{(a)y} z_a^x, \quad \mathbf{x} \rightarrow +\infty, \\ \psi_{x,y} &\sim A \sum_{b=1}^{N^B} \mathcal{J}_{\tilde{a}b}^{\tilde{A}B} a_{(b)y} z_b^x, \quad \mathbf{x} \rightarrow -\infty. \end{aligned} \quad (37a)$$

Analogously, corresponding to (37a), at the starred sites in the leads, the total function is given by

$$\begin{aligned} \psi_{x,y}^* &\sim A a_{(\tilde{a})y}^* z_{\tilde{a}}^x + A \sum_{a=1}^{N^A} \mathcal{J}_{\tilde{a}a}^{\tilde{A}A} a_{(a)y}^* z_a^x, \quad \mathbf{x} \rightarrow +\infty, \\ \psi_{x,y}^* &\sim A \sum_{b=1}^{N^B} \mathcal{J}_{\tilde{a}b}^{\tilde{A}B} a_{(b)y}^* z_b^x, \quad \mathbf{x} \rightarrow -\infty. \end{aligned} \quad (37b)$$

The velocity  $v$  of an electronic wave mode with wave number  $\xi$  is given by  $d\mathcal{E} = \hbar v(\xi) d\xi$ , following the exposition provided in [68]. Using the asymptotic analysis presented

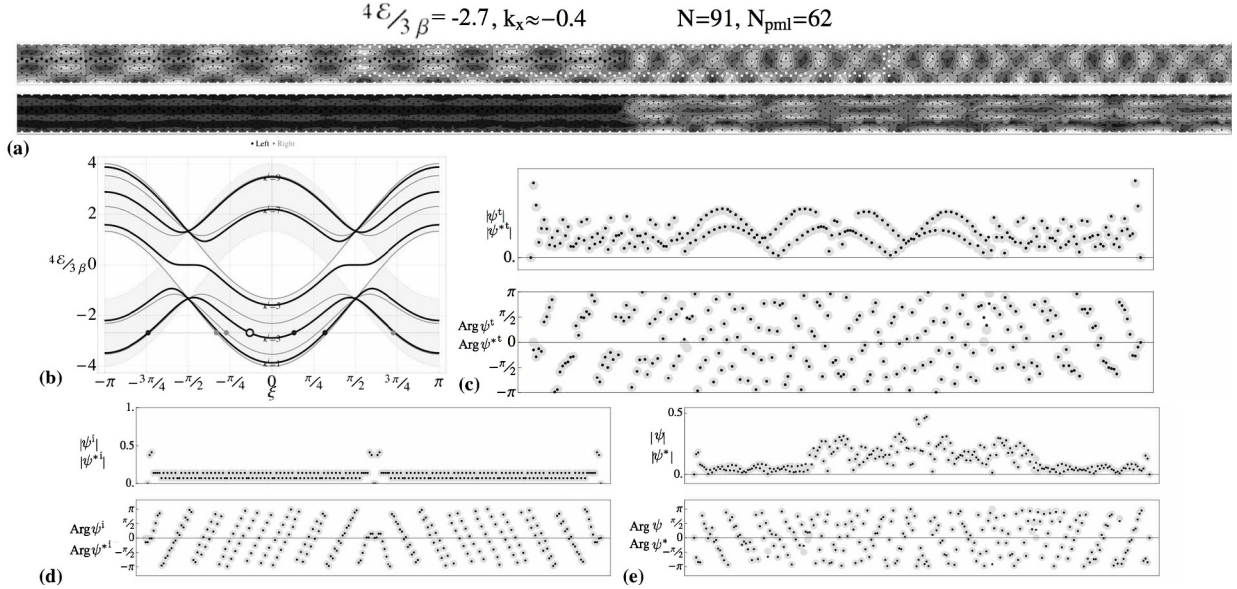


**Fig. 7.** Incidence from nanoribbon of an even mode when the width of  $\mathcal{H}_\pm^\otimes$  is  $N = 6$ . All other details are same as those provided in the caption of Figure 6.

above in Section 5, it is prudent to define the coefficients in above expression, so called reflection and transmission amplitudes [68], respectively, as

$$\tau_{a\bar{a}}^{A\bar{A}} = \mathcal{T}_{\bar{a}a}^{\bar{A}A} \sqrt{\frac{|v_a|}{|v_{\bar{a}}|}}, \quad \tau_{b\bar{b}}^{B\bar{B}} = \mathcal{T}_{\bar{b}b}^{\bar{B}B} \sqrt{\frac{|v_b|}{|v_{\bar{b}}|}}. \quad (38)$$

Hence, based on (37a) and (37b), the right ( $\mathfrak{s} = A$ ) and the left ( $\mathfrak{s} = B$ ) scattering states, respectively, are given by

$$\begin{aligned} \psi_a^A &\rightarrow \psi_{\bar{a}} + \sum_{a=1}^{N^A} \tau_{a\bar{a}}^{A\bar{A}} \sqrt{\frac{|v_{\bar{a}}|}{|v_a|}} \psi_a, \\ \psi_{\bar{a}}^{*A} &\rightarrow \psi_{\bar{a}}^* + \sum_{a=1}^{N^A} \tau_{a\bar{a}}^{A\bar{A}} \sqrt{\frac{|v_{\bar{a}}|}{|v_a|}} \psi_a^*, \\ \psi_b^B &\rightarrow \sum_{b=1}^{N^B} \tau_{b\bar{b}}^{B\bar{B}} \sqrt{\frac{|v_{\bar{b}}|}{|v_b|}} \psi_b, \\ \psi_{\bar{b}}^{*B} &\rightarrow \sum_{b=1}^{N^B} \tau_{b\bar{b}}^{B\bar{B}} \sqrt{\frac{|v_{\bar{b}}|}{|v_b|}} \psi_b^*. \end{aligned} \quad (39)$$

Also for the incidence from the ribbon portion, ahead and behind the junction, respectively, assuming  $z_P$  corresponds to the index  $\tilde{b}$  (i.e.,  $z_P = z_{\tilde{b}}$ ) in (33), in the spirit of (38) it is natural to define

$$\tau_{a\tilde{b}}^{A\tilde{B}} = \mathcal{T}_{\tilde{b}a}^{\tilde{B}A} \sqrt{\frac{|v_a|}{|v_{\tilde{b}}|}}, \quad \tau_{b\tilde{b}}^{B\tilde{B}} = \mathcal{T}_{\tilde{b}b}^{\tilde{B}B} \sqrt{\frac{|v_b|}{|v_{\tilde{b}}|}}, \quad (40)$$

while, the far-field expressions corresponding to (33) can be expressed as

$$\begin{aligned} \psi_{x,y} &\sim A \sum_{a=1}^{N^A} \mathcal{T}_{\tilde{b}a}^{\tilde{B}A} a_{(a)y} z_a^x, \quad \mathbf{x} \rightarrow +\infty, \\ \psi_{x,y} &\sim A a_{(\tilde{b})y} z_{\tilde{b}}^x + A \sum_{b=1}^{N^B} \mathcal{T}_{\tilde{b}b}^{\tilde{B}B} a_{(b)y} z_b^x, \quad \mathbf{x} \rightarrow -\infty, \end{aligned} \quad (41a)$$

and

$$\begin{aligned} \psi_{x,y}^* &\sim A \sum_{a=1}^{N^A} \mathcal{T}_{\tilde{b}a}^{\tilde{B}A} a_{(a)y}^* z_a^x, \quad \mathbf{x} \rightarrow +\infty, \\ \psi_{x,y}^* &\sim A a_{(\tilde{b})y}^* z_{\tilde{b}}^x + A \sum_{b=1}^{N^B} \mathcal{T}_{\tilde{b}b}^{\tilde{B}B} a_{(b)y}^* z_b^x, \quad \mathbf{x} \rightarrow -\infty \end{aligned} \quad (41b)$$

Both above equations in (41) can be re-written in the manner of (39) as

$$\begin{aligned} \psi_b^A &\rightarrow \sum_{a=1}^{N^A} \tau_{ab}^{A\tilde{B}} \sqrt{\frac{|v_{\tilde{b}}|}{|v_a|}} \psi_a, \\ \psi_{\tilde{b}}^{*A} &\rightarrow \sum_{a=1}^{N^A} \tau_{ab}^{A\tilde{B}} \sqrt{\frac{|v_{\tilde{b}}|}{|v_a|}} \psi_a^*, \\ \psi_b^B &\rightarrow \psi_{\tilde{b}} + \sum_{b=1}^{N^B} \tau_{b\tilde{b}}^{B\tilde{B}} \sqrt{\frac{|v_{\tilde{b}}|}{|v_b|}} \psi_b, \\ \psi_{\tilde{b}}^{*B} &\rightarrow \psi_{\tilde{b}}^* + \sum_{b=1}^{N^B} \tau_{b\tilde{b}}^{B\tilde{B}} \sqrt{\frac{|v_{\tilde{b}}|}{|v_b|}} \psi_b^*, \end{aligned} \quad (42)$$

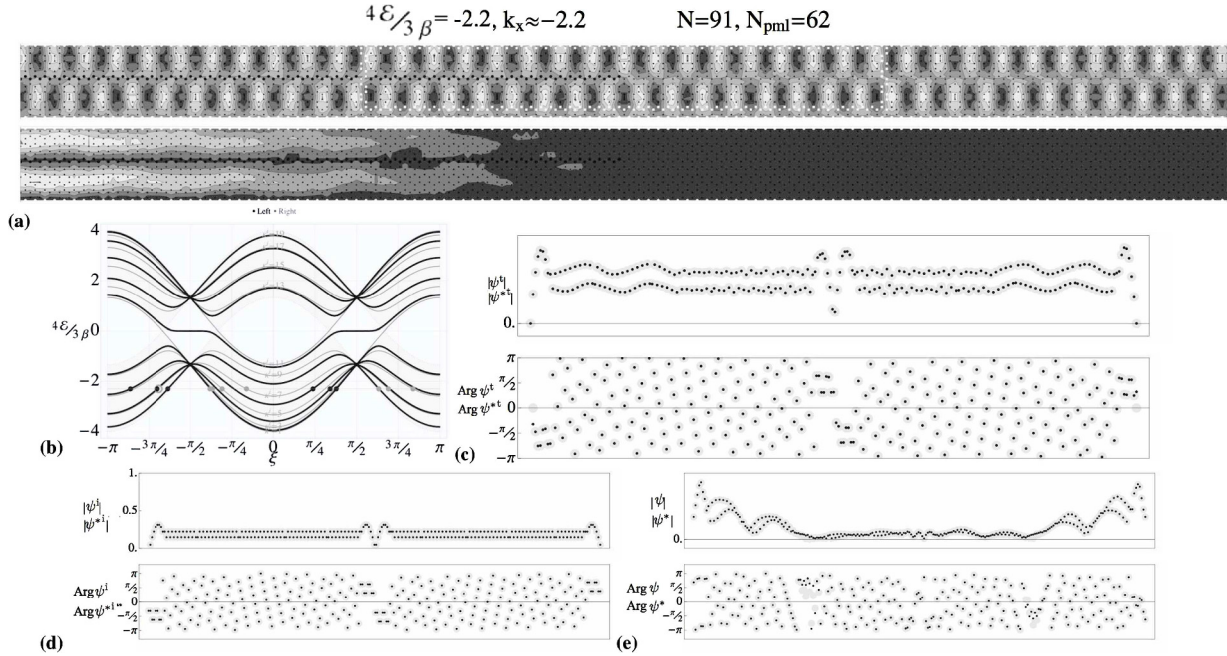


**Fig. 8.** Incidence from nanotube ( $N = 10$ ) corresponding to the same energy as in Figure 6 but  $|\kappa| \in (\frac{1}{2}\pi, \pi)$ . All other details are same as those provided in the caption of Figure 6.

to express the right ( $\mathfrak{s} = A$ ) and the left ( $\mathfrak{s} = A$ ) scattering states, respectively.

The notational advantage of the expressions (39) and (42) lies in their application in the specification of the scattering matrix associated with the junction structure studied in this paper. Indeed, the general description of the incoming electronic state is provided by the form [68]

$$\psi(\mathcal{E}) = \sum_{\tilde{a}=1}^{N^A} \frac{l_{\tilde{a}}^A}{\sqrt{|v_{\tilde{a}}^A|}} \psi_{\tilde{a}} + \sum_{\tilde{b}=1}^{N^B} \frac{l_{\tilde{b}}^B}{\sqrt{|v_{\tilde{b}}^B|}} \psi_{\tilde{b}}. \quad (43)$$

In view of the analysis presented so far in this paper, the relations

$$\begin{aligned} O_A^a &\equiv \sum_{\tilde{a}=1}^{N^A} l_{\tilde{a}}^A \tau_{\tilde{a}\tilde{a}}^{A\tilde{A}} + \sum_{\tilde{b}=1}^{N^B} l_{\tilde{b}}^B \tau_{\tilde{a}\tilde{b}}^{A\tilde{B}}, \\ O_B^b &\equiv \sum_{\tilde{a}=1}^{N^A} l_{\tilde{a}}^A \tau_{\tilde{b}\tilde{a}}^{B\tilde{A}} + \sum_{\tilde{b}=1}^{N^B} l_{\tilde{b}}^B \tau_{\tilde{b}\tilde{b}}^{B\tilde{B}}, \end{aligned} \quad (44)$$

lead to the desired asymptotic form of the solution of the transmission problem (using (39) and (42)) as

$$\begin{cases} \sum_{\tilde{a}=1}^{N^A} \sqrt{|v_{\tilde{a}}^A|}^{-1} l_{\tilde{a}}^A \psi_{\tilde{a}} + \sum_{\tilde{a}=1}^{N^A} \sqrt{|v_{\tilde{a}}^A|}^{-1} O_A^a \psi_a \\ \text{on the tubular side,} \\ \sum_{\tilde{b}=1}^{N^B} \sqrt{|v_{\tilde{b}}^B|}^{-1} l_{\tilde{b}}^B \psi_{\tilde{b}} + \sum_{\tilde{b}=1}^{N^B} \sqrt{|v_{\tilde{b}}^B|}^{-1} O_B^b \psi_b \\ \text{on the ribbon side.} \end{cases} \quad (45)$$

By noting that deep in both B and A leads (as schematically shown in Fig. 5) the entities  $\psi_a, \psi_a^*, \psi_b, \psi_b^*$  represent an electronic wavemode moving outward from the nanojunction, while  $\psi_{\tilde{a}}, \psi_{\tilde{a}}^*, \psi_{\tilde{b}}, \psi_{\tilde{b}}^*$  represent an electronic wavemode moving inward towards the nanojunction, above equation (44) defines a linear relation between the outgoing flux amplitudes  $O_{A,B}^{a,b}$  to the incoming flux amplitudes  $l_{A,B}^{\tilde{a},\tilde{b}}$ . The same relation can be further written in a matrix form as

See equation (46) next page

where the coefficient matrix, denoted by  $\mathbf{S}$ , is called the  $S$  matrix given that  $N^A$  channels in the lead A and  $N^B$  channels in the lead B are available. In a shorter and traditional form, the  $S$ -matrix can be also expressed as

$$\mathbf{S} = \begin{bmatrix} \mathbf{r}^{N^A \times N^A} & \tilde{\mathbf{t}}^{N^A \times N^B} \\ \mathbf{t}^{N^B \times N^A} & \tilde{\mathbf{r}}^{N^B \times N^B} \end{bmatrix}, \quad (47)$$

where  $\mathbf{r} = [\tau_{ij}^{A\tilde{A}}]$ ,  $\tilde{\mathbf{r}} = [\tau_{ij}^{B\tilde{B}}]$ ,  $\tilde{\mathbf{t}} = [\tau_{ij}^{A\tilde{B}}]$ ,  $\mathbf{t} = [\tau_{ij}^{B\tilde{A}}]$ . The properties of the  $S$ -matrix are standard. In particular, the  $\mathbf{S}$  matrix is unitary as a consequence of expressing particle flux conservation, i.e.,

$$\mathbf{S}\mathbf{S}^\dagger = \mathbf{S}^\dagger\mathbf{S} = \mathbf{1}. \quad (48)$$

Hence, the form of (47) implies

$$\mathbf{r}\mathbf{r}^\dagger + \tilde{\mathbf{t}}\tilde{\mathbf{t}}^\dagger = \mathbf{r}^\dagger\mathbf{r} + \tilde{\mathbf{t}}^\dagger\tilde{\mathbf{t}} = \mathbf{1}_{N^A \times N^A}, \quad (49a)$$

$$\mathbf{t}\mathbf{t}^\dagger + \tilde{\mathbf{r}}\tilde{\mathbf{r}}^\dagger = \mathbf{t}^\dagger\mathbf{t} + \tilde{\mathbf{r}}^\dagger\tilde{\mathbf{r}} = \mathbf{1}_{N^B \times N^B}, \quad (49b)$$

$$\mathbf{r}\mathbf{t}^\dagger + \tilde{\mathbf{r}}\tilde{\mathbf{t}}^\dagger = \mathbf{r}^\dagger\tilde{\mathbf{t}} + \mathbf{t}^\dagger\tilde{\mathbf{r}} = \mathbf{0}_{N^A \times N^B}, \quad (49c)$$

$$\begin{bmatrix} \mathbf{O}_A^1 \\ \mathbf{O}_A^2 \\ \vdots \\ \mathbf{O}_A^{N^A} \\ \mathbf{O}_B^1 \\ \mathbf{O}_B^2 \\ \vdots \\ \mathbf{O}_B^{N^B} \end{bmatrix} = \begin{bmatrix} \tau_{11}^{A\bar{A}} & \cdots & \tau_{1N^A}^{A\bar{A}} & \tau_{11}^{A\bar{B}} & \cdots & \tau_{1N^B}^{A\bar{B}} \\ \tau_{21}^{A\bar{A}} & \ddots & & \tau_{21}^{A\bar{B}} & \tau_{22}^{A\bar{B}} & \vdots \\ \vdots & & \ddots & \vdots & & \ddots \\ \tau_{N^A 1}^{A\bar{A}} & \cdots & \tau_{N^A N^A}^{A\bar{A}} & \tau_{N^A 1}^{A\bar{B}} & \cdots & \tau_{N^A N^B}^{A\bar{B}} \\ \tau_{11}^{B\bar{A}} & \cdots & \tau_{1N^A}^{B\bar{A}} & \tau_{11}^{B\bar{B}} & \cdots & \tau_{1N^B}^{B\bar{B}} \\ \tau_{21}^{B\bar{A}} & \ddots & & \tau_{21}^{B\bar{B}} & \tau_{22}^{B\bar{B}} & \vdots \\ \vdots & & \ddots & \vdots & & \ddots \\ \tau_{N^B 1}^{B\bar{A}} & \cdots & \tau_{N^B N^A}^{B\bar{A}} & \tau_{N^B 1}^{B\bar{B}} & \cdots & \tau_{N^B N^B}^{B\bar{B}} \end{bmatrix} \begin{bmatrix} \mathbf{1}_A^1 \\ \mathbf{1}_A^2 \\ \vdots \\ \mathbf{1}_A^{N^A} \\ \mathbf{1}_B^1 \\ \mathbf{1}_B^2 \\ \vdots \\ \mathbf{1}_B^{N^B} \end{bmatrix}, \quad (46)$$

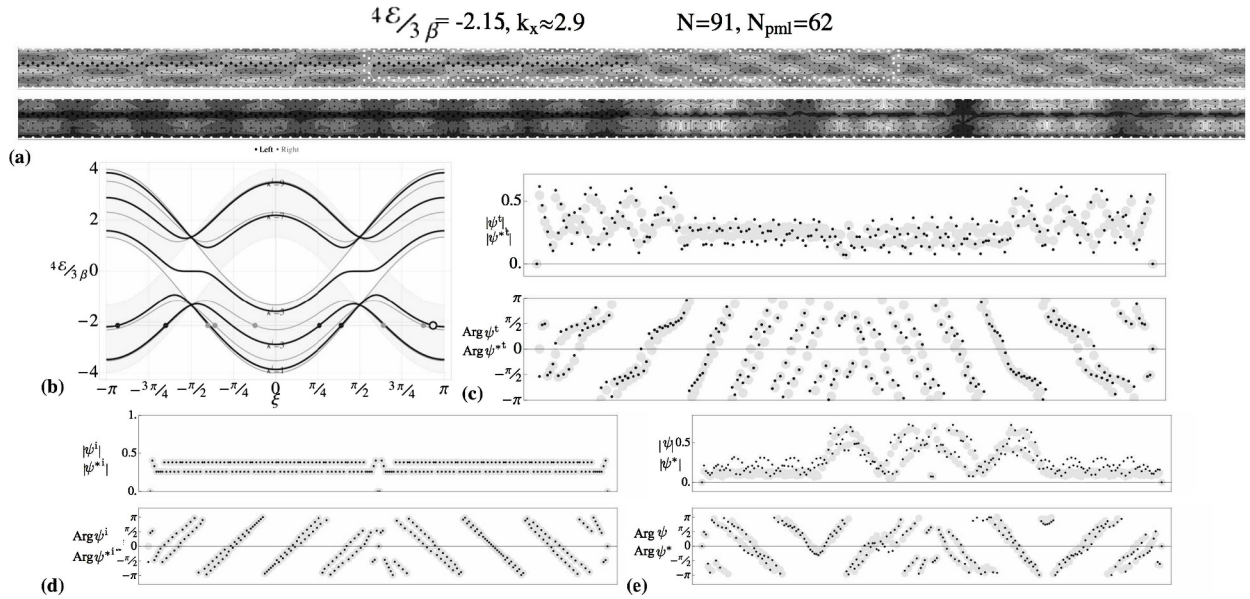


**Fig. 9.** Incidence from nanoribbon corresponding to the same energy as in Figure 7 but  $|\kappa| \in (\frac{1}{2}\pi, \pi)$  (and  $N = 6$ ). All other details are same as those provided in the caption of Figure 6.

$$\mathbf{t}\mathbf{r}^\dagger + \widetilde{\mathbf{r}}\widetilde{\mathbf{t}}^\dagger = \widetilde{\mathbf{t}}^\dagger\mathbf{r} + \widetilde{\mathbf{r}}^\dagger\mathbf{t} = \mathbf{0}_{N^B \times N^A}, \quad (49d)$$

where  $\mathbf{1}$  and  $\mathbf{0}$  are the unit matrix and a matrix with all elements zero, respectively, with dimensions given by the subscripts. Since the assumed system is conservative ( $\mathcal{E} \simeq \mathcal{E} + i0$ ), it is also found that  $\mathbf{t}_{N^B \times N^A} = (\mathbf{t}_{N^A \times N^B})^\top$ , i.e.,  $\mathbf{S}$  is symmetric. The relations (49) motivate a further analysis of the modulus of each element of the scattering matrix. Indeed such an exercise is vital for the determination of the reflection and transmission coefficient for a wave incident from either side of the junction. The large set of above relations given by (49) between the transmission and reflection probabilities are studied further below; in particular (49a) and (49b).

The reflection coefficient (resp. transmission coefficient) is obtained by taking the diagonal entries of  $\mathbf{r}\mathbf{r}^\dagger$  for the incidence from the nanotube and  $\widetilde{\mathbf{r}}\widetilde{\mathbf{r}}^\dagger$  for the incidence from the nanoribbon where  $\mathbf{r} = [\tau_{ij}^{A\bar{A}}]$  and  $\widetilde{\mathbf{r}} = [\tau_{ij}^{B\bar{B}}]$  (resp.  $\mathbf{t}\mathbf{t}^\dagger$  for the incidence from the nanotube and  $\widetilde{\mathbf{t}}\widetilde{\mathbf{t}}^\dagger$  for the incidence from the nanoribbon, where  $\widetilde{\mathbf{t}} = [\tau_{ij}^{A\bar{B}}]$ ,  $\mathbf{t} = [\tau_{ij}^{B\bar{A}}]$ ). Using the energy band relation  $\hbar v(\xi) := \frac{\partial \mathcal{E}}{\partial \xi}$  can

be found. The detailed expression of the transmission coefficient for incident wave corresponding to  $\bar{\mathbf{b}}$  from the “lead” B into the transmitted wave corresponding to  $\mathbf{a}$  in “lead” A is found using the three relations (38), (32), and (37), as well as (40), (33), and (41).

For example, consider the coefficient  $|\tau_{\bar{\mathbf{a}}\bar{\mathbf{a}}}^{A\bar{A}}|^2$  and  $|\tau_{\bar{\mathbf{b}}\bar{\mathbf{b}}}^{A\bar{A}}|^2$  for illustration. Using (38)<sub>1</sub>,

$$\begin{aligned} |\tau_{\bar{\mathbf{a}}\bar{\mathbf{a}}}^{A\bar{A}}|^2 &= -\frac{v(\xi_{\bar{\mathbf{a}}})}{v(\xi_{\bar{\mathbf{a}}})} \mathcal{T}_{\bar{\mathbf{a}}\bar{\mathbf{a}}}^{\bar{A}A} \overline{\mathcal{T}_{\bar{\mathbf{a}}\bar{\mathbf{a}}}^{\bar{A}A}} \\ &= 2 \times \frac{1}{4} \frac{v(\xi)}{4 - v(\xi_P)} \left| \frac{\mathcal{N}_+(z_P)}{\widehat{\mathcal{D}}_+(z_P)} \right|^2 \frac{|\mathbf{a}^*(\kappa^i)_1|^2}{|\mathbf{a}^*(\kappa_z)_1|^2} \\ &\quad \times \left| \frac{\widehat{\mathcal{D}}_+(z)}{\mathcal{N}'_+(z)} \right|^2 \left| \frac{1}{z - z_P} \right|^2, \end{aligned} \quad (50)$$

where the factor of 2 appears due to analogous expression on the replicated lattice structure. With the analytical details provided in Appendix E.1, for all  $\mathbf{a}$  and  $\bar{\mathbf{a}}$  involving

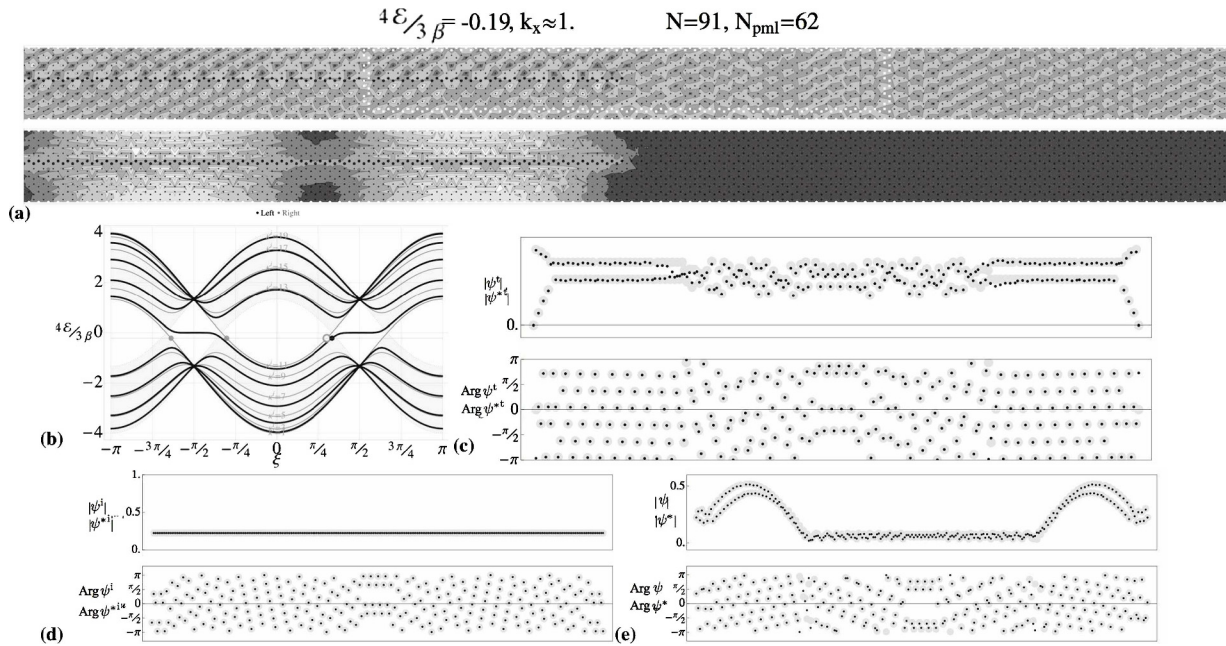


**Fig. 10.** Incidence from nanotube ( $N = 10$ ) for energy close to the Dirac cone location. All other details are same as those provided in the caption of Figure 6.

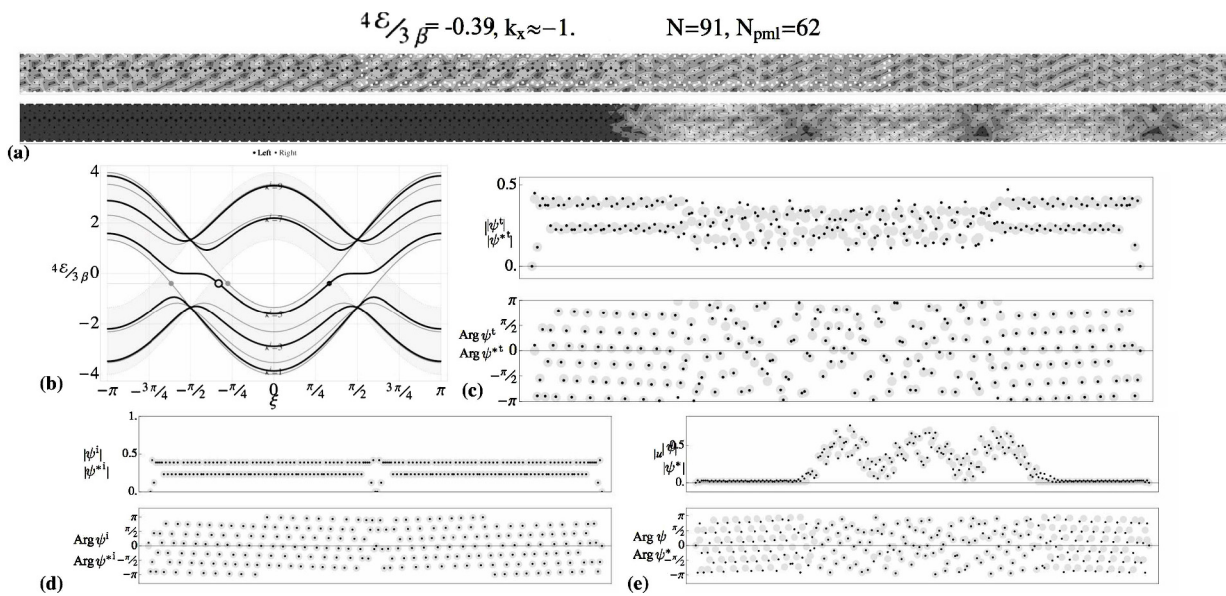


**Fig. 11.** Incidence from nanoribbon ( $N = 6$ ) for energy close to the Dirac cone location. All other details are same as those provided in the caption of Figure 6.

even modes, it is found that

$$|\tau_{a\bar{a}}^{A\bar{A}}|^2 = \frac{1}{2} \widehat{C}_{\bar{a}} \frac{z_{\bar{a}}}{(z_a - z_{\bar{a}})^2} \frac{\overline{\mathcal{N}_-(z_a) \widehat{\mathcal{D}}_+(z_a)}}{\widehat{\mathcal{D}}_-(z_a) \mathcal{N}'_+(z_a)}, \quad (51)$$

where

$$\widehat{C}_{\bar{a}} = \frac{z_{\bar{a}} \widehat{\mathcal{D}}_-(z_{\bar{a}}) \mathcal{N}_+(z_{\bar{a}})}{\mathcal{N}'_-(z_{\bar{a}}) \widehat{\mathcal{D}}_+(z_{\bar{a}})}. \quad (52)$$

Also, using (38)<sub>2</sub>,

$$|\tau_{b\bar{a}}^{B\bar{A}}|^2 = \frac{1}{2} \widehat{C}_{\bar{a}} \frac{z_{\bar{a}}}{(z_b - z_{\bar{a}})^2} \frac{\overline{\mathcal{N}_-(z_b) \widehat{\mathcal{D}}_+(z_b)}}{\widehat{\mathcal{D}}_-(z_b) \mathcal{N}'_+(z_b)}. \quad (53)$$

Analogous expressions hold for  $|\tau_{a\bar{a}}^{A\bar{A}}|^2$  and  $|\tau_{b\bar{a}}^{B\bar{A}}|^2$  involving the indices a and b corresponding to the odd symmetry. For the incident modes of odd symmetry,  $z_{\bar{a}} \mapsto -z_{\bar{a}}$  is needed.

Repeating the analysis for the wave incidence from the ribbon side (to account for the reflection into the ribbon and transmission into the tubular side), it is found that for all  $\mathbf{a}$ ,  $\mathbf{b}$ , and  $\tilde{\mathbf{b}}$  of even symmetry,

$$|\tau_{\mathbf{a}\tilde{\mathbf{b}}}^{\mathbf{A}\tilde{\mathbf{B}}}|^2 = \frac{1}{2} \hat{\mathcal{C}}_{\tilde{\mathbf{b}}} \frac{z_{\tilde{\mathbf{b}}}}{(z_{\mathbf{a}} - z_{\tilde{\mathbf{b}}})^2} \frac{\overline{\mathcal{N}_-(z_{\mathbf{a}}) \hat{\mathcal{D}}_+(z_{\mathbf{a}})}}{\hat{\mathcal{D}}_-(z_{\mathbf{a}}) \mathcal{N}'_+(z_{\mathbf{a}})}, \quad (54)$$

$$|\tau_{\mathbf{b}\tilde{\mathbf{b}}}^{\mathbf{B}\tilde{\mathbf{B}}}|^2 = \frac{1}{2} \hat{\mathcal{C}}_{\tilde{\mathbf{b}}} \frac{z_{\tilde{\mathbf{b}}}}{(z_{\mathbf{b}} - z_{\tilde{\mathbf{b}}})^2} \frac{\overline{\mathcal{N}_-(z_{\mathbf{b}}) \hat{\mathcal{D}}_+(z_{\mathbf{b}})}}{\hat{\mathcal{D}}'_-(z_{\mathbf{b}}) \mathcal{N}_+(z_{\mathbf{b}})}. \quad (55)$$

where (as counterpart of (52))

$$\hat{\mathcal{C}}_{\tilde{\mathbf{b}}} = \frac{z_{\tilde{\mathbf{b}}} \hat{\mathcal{D}}_-(z_{\tilde{\mathbf{b}}}) \mathcal{N}_+(z_{\tilde{\mathbf{b}}})}{\overline{\mathcal{N}_-(z_{\tilde{\mathbf{b}}}) \hat{\mathcal{D}}'_+(z_{\tilde{\mathbf{b}}})}}. \quad (56)$$

Analogous expressions hold for  $|\tau_{\mathbf{a}\tilde{\mathbf{b}}}^{\mathbf{A}\tilde{\mathbf{B}}}|^2$  and  $|\tau_{\mathbf{b}\tilde{\mathbf{b}}}^{\mathbf{B}\tilde{\mathbf{B}}}|^2$  involving the indices  $\mathbf{a}$  and  $\mathbf{b}$  corresponding to the odd symmetry. For the incident modes of odd symmetry,  $z_{\tilde{\mathbf{b}}} \mapsto -z_{\tilde{\mathbf{b}}}$  mapping is used.

For a wave incident from the tubular side, the transmittance is given by the expression

$$\mathcal{J}_{\mathbf{B}\leftarrow\mathbf{A}}^{\tilde{\mathbf{a}}} = \sum_{\tilde{\mathbf{b}}=1}^{N^{\mathbf{B}}} |\tau_{\tilde{\mathbf{b}}\tilde{\mathbf{a}}}^{\tilde{\mathbf{B}}\tilde{\mathbf{A}}}|^2, \quad (57)$$

and the reflectance is  $\mathcal{R}_{\mathbf{B}\leftarrow\mathbf{A}}^{\tilde{\mathbf{a}}} = 1 - \mathcal{J}_{\mathbf{B}\leftarrow\mathbf{A}}^{\tilde{\mathbf{a}}}$ . On the other hand, for a wave incident from the ribbon side, the transmittance is given by the expression

$$\mathcal{J}_{\mathbf{B}\rightarrow\mathbf{A}}^{\tilde{\mathbf{b}}} = \sum_{\tilde{\mathbf{a}}=1}^{N^{\mathbf{A}}} |\tau_{\tilde{\mathbf{a}}\tilde{\mathbf{b}}}^{\tilde{\mathbf{A}}\tilde{\mathbf{B}}}|^2, \quad (58)$$

and the reflectance is  $\mathcal{R}_{\mathbf{B}\rightarrow\mathbf{A}}^{\tilde{\mathbf{b}}} = 1 - \mathcal{J}_{\mathbf{B}\rightarrow\mathbf{A}}^{\tilde{\mathbf{b}}}$ .

A graphical illustration of the transmittance (57) and (58) is provided in Figure 12, where the part (a) (resp. (b)) gives the results for incidence from the tube (resp. ribbon). Notice that the darker (resp. lighter) shade of the energy bands (for even modes) corresponds to the portion for the wave incidence (resp. reflection). Naturally, the union of the reflected and incident parts completes the energy bands for each portion. Observe that the energy bands for incident waves are not the same as those for the transmitted waves by an inspection of the left parts of Figure 12a vs. Figure 12b; the latter has been obtained by changing the direction of incidence against that in Figure 12a. Figure 13 complements the results of Figure 12 in the way that it presents the reflectance corresponding to the same choice of parameters, however, the dependence is shown with respect to the incident wave number  $\xi$  in place of the energy level  $\mathcal{E}$ . In Figure 13a the incidence is from tubular side while in Figure 13b the wave is incident from the ribbon. These results have been validated against the relevant calculation based on the numerical solution

corresponding to Figures 6–11 though corresponding data points are not shown in Figures 12 and 13 in order to maintain the clarity for the provision of analytically obtained curves. The gray numbered curves are symmetrically related to the white numbered curves, the correspondence with the energy bands shown in Figure 12 depicts the same symmetry transformation. Although the energy bands for only even modes are shown in Figure 12, the transmittance for the incident even vs. transmitted odd modes, incident odd vs. transmitted even modes, as well as incident odd vs. transmitted odd modes, remains the same in view of the relation between the even vs. odd symmetry as explained in Appendix B.

## 7 Conductance

It is well known that the equations (39) and (42) (based on (32) and (33)), form the basis of the *Landauer–Büttiker formalism* (or rather a viewpoint of conduction [43,44]) as they play a crucial role in calculation of the electrical conductance from the asymptotic form (provided by the former both expressions) of the scattering states [68,69]. In the present two terminal case, the Landauer–Büttiker formalism relates the scattering matrix to the conductance of the sample (with two terminals) as  $\mathcal{G}$  ( $= \mathcal{G}_{\mathbf{B}\leftarrow\mathbf{A}} = \mathcal{G}_{\mathbf{B}\rightarrow\mathbf{A}}$ , by the properties of the  $S$ -matrix). Recall that the elements of  $\mathcal{Z}_{\mathbf{A}}^+$  (resp.  $\mathcal{Z}_{\mathbf{A}}^-$ ) are indexed by  $\mathbf{a}$  (resp.  $\tilde{\mathbf{a}}$ ) with a range  $1 \dots N^{\mathbf{A}}$ , while the elements of  $\mathcal{Z}_{\mathbf{B}}^-$  (resp.  $\mathcal{Z}_{\mathbf{B}}^+$ ) are indexed by  $\mathbf{b}$  (resp.  $\tilde{\mathbf{b}}$ ) ranging from 1 to  $N^{\mathbf{B}}$ . Following [70], the conductance  $\mathcal{G}$  (in the unit of quantum conductance  $\mathcal{G}_Q$  [70–72]) is given by the sum of transmission coefficients for all incident wave numbers, i.e.,  $\mathcal{G} = \mathcal{G}_{\mathbf{B}\leftarrow\mathbf{A}} = \sum_{\tilde{\mathbf{a}}=1}^{N^{\mathbf{A}}} \mathcal{J}_{\mathbf{B}\leftarrow\mathbf{A}}^{\tilde{\mathbf{a}}} = \mathcal{G}_{\mathbf{B}\rightarrow\mathbf{A}} = \sum_{\tilde{\mathbf{b}}=1}^{N^{\mathbf{B}}} \mathcal{J}_{\mathbf{B}\rightarrow\mathbf{A}}^{\tilde{\mathbf{b}}}$  using the expressions (57) and (58) in terms of the reflection and transmission moduli. For example, using (58),

$$\begin{aligned} \mathcal{G}_{\mathbf{B}\rightarrow\mathbf{A}} &= \sum_{\tilde{\mathbf{a}}=1}^{N^{\mathbf{A}}} \sum_{\tilde{\mathbf{b}}=1}^{N^{\mathbf{B}}} |\tau_{\tilde{\mathbf{b}}\tilde{\mathbf{a}}}^{\tilde{\mathbf{B}}\tilde{\mathbf{A}}}|^2 = \sum_{\tilde{\mathbf{a}}=1}^{N^{\mathbf{A}}} \sum_{\tilde{\mathbf{b}}=1}^{N^{\mathbf{B}}} \frac{|v_{\tilde{\mathbf{a}}}^{\mathbf{A}}|}{|v_{\tilde{\mathbf{b}}}^{\mathbf{B}}|} |\mathcal{J}_{\tilde{\mathbf{a}}\tilde{\mathbf{b}}}^{\mathbf{A}\tilde{\mathbf{B}}}|^2 \\ &= -2 \sum_{\tilde{\mathbf{a}}=1}^{\frac{1}{2}N^{\mathbf{A}}} \sum_{\tilde{\mathbf{b}}=1}^{\frac{1}{2}N^{\mathbf{B}}} \frac{\overline{\mathcal{D}}_-(z_{\tilde{\mathbf{a}}}) \mathcal{N}_+(z_{\tilde{\mathbf{a}})}}{\mathcal{N}'_-(z_{\tilde{\mathbf{a}}}) \hat{\mathcal{D}}_+(z_{\tilde{\mathbf{a}}})} \frac{\overline{\mathcal{D}}_-(z_{\tilde{\mathbf{b}}}) \hat{\mathcal{D}}_+(z_{\tilde{\mathbf{b}}})}{\hat{\mathcal{D}}'_-(z_{\tilde{\mathbf{b}}}) \mathcal{N}_+(z_{\tilde{\mathbf{b}}})} \frac{z_{\tilde{\mathbf{a}}} z_{\tilde{\mathbf{b}}}}{|z_{\tilde{\mathbf{a}}} - z_{\tilde{\mathbf{b}}}|^2}, \end{aligned} \quad (59)$$

and based on (57),

$$\begin{aligned} \mathcal{G}_{\mathbf{B}\leftarrow\mathbf{A}} &= -2 \sum_{\tilde{\mathbf{a}}=1}^{\frac{1}{2}N^{\mathbf{A}}} \sum_{\tilde{\mathbf{b}}=1}^{\frac{1}{2}N^{\mathbf{B}}} \frac{\overline{\mathcal{N}_-(z_{\tilde{\mathbf{a}}}) \hat{\mathcal{D}}_+(z_{\tilde{\mathbf{a}}})}}{\hat{\mathcal{D}}_-(z_{\tilde{\mathbf{a}}}) \mathcal{N}'_+(z_{\tilde{\mathbf{a}}})} \frac{\overline{\mathcal{D}}_-(z_{\tilde{\mathbf{b}}}) \mathcal{N}_+(z_{\tilde{\mathbf{b}}})}{\mathcal{N}_-(z_{\tilde{\mathbf{b}}}) \hat{\mathcal{D}}'_+(z_{\tilde{\mathbf{b}}})} \frac{z_{\tilde{\mathbf{a}}} z_{\tilde{\mathbf{b}}}}{|z_{\tilde{\mathbf{a}}} - z_{\tilde{\mathbf{b}}}|^2}. \end{aligned} \quad (60)$$

Observe that the expression (59) and (60) is simply four times the conductance *restricted to only even modes*.

The ballistic conductance  $\mathcal{G}^{\text{ball}}$  (in the unit of quantum conductance  $\mathcal{G}_Q$  [70–72]) is equal to the number of channels on the left, which are transmitted to the right (and is

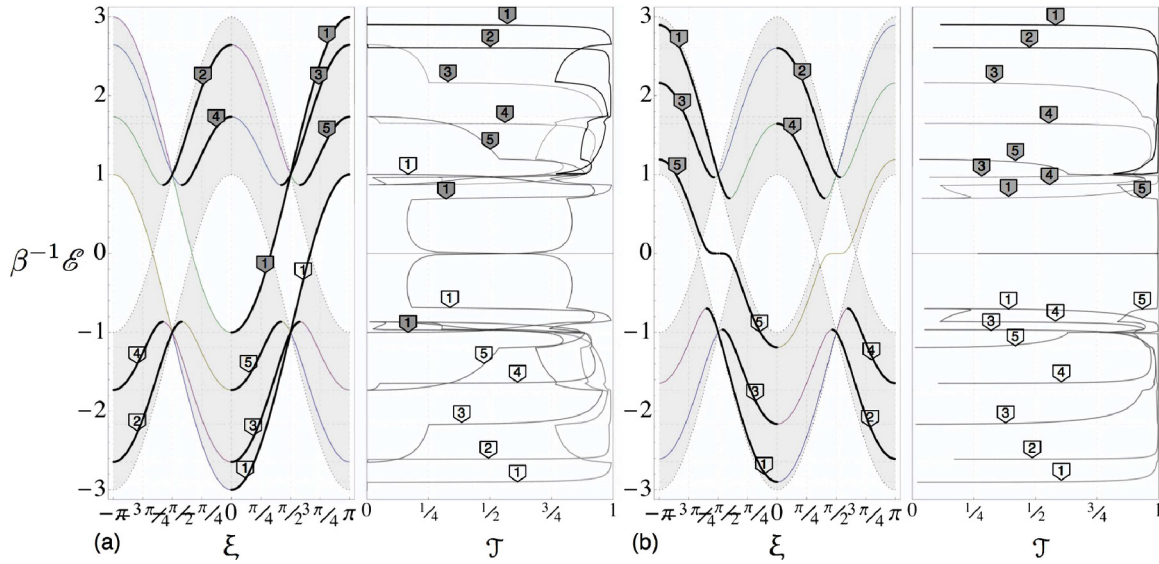


**Fig. 12.** Transmittance  $\mathcal{T}$  for incidence from tube for  $N = 6$ . The darker curves for transmittance  $\mathcal{T}$  (equal to  $\mathcal{T}_{B \leftarrow A}^{\bar{5}}$  on left pair (a) and  $\mathcal{T}_{B \rightarrow A}^{\bar{5}}$  on the right (b)) correspond to incident (even mode) wave with wavenumber lying on the higher energy bands. The vertical (energy) axis demonstrates the correspondence between (even mode) energy bands for the two parts of the junction and critical values attained in transmittance. The lighter (resp. darker) shade of the energy bands on the left plot of each pair corresponds to the transmitted (reflected) part.

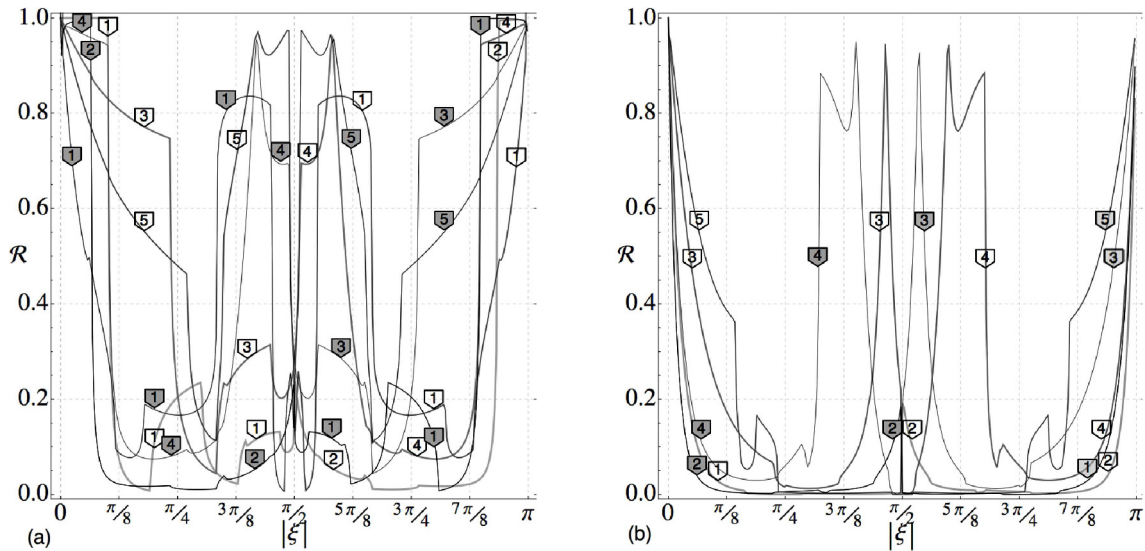


**Fig. 13.** Reflectance  $\mathcal{R}$  for the junction of honeycomb lattice ribbons ( $N = 6$ ). (a) Incidence from tube, i.e.,  $\mathcal{R}_{B \leftarrow A}^{\bar{5}} (= 1 - \mathcal{T}_{B \leftarrow A}^{\bar{5}})$ . (b) Incidence from the lattice ribbon, i.e.,  $\mathcal{R}_{B \rightarrow A}^{\bar{5}} (= 1 - \mathcal{T}_{B \rightarrow A}^{\bar{5}})$ . The critical values attained in reflectance  $\mathcal{R}$  correspond to the critical values of the energy band [62]. The curve labels in (a) and (b) correspond to Figures 12a and 12b, respectively.

also equal to the number of channels on the right, which are transmitted to the left). This can be expressed as [70] (Eq. (11.1))

$$\mathcal{G}^{\text{ball}} = \min\{N^A, N^B\}, \tag{61}$$

for the present structure shown in Figure 1.

A graphical illustration of the dependence of  $\mathcal{G}^{\text{ball}}$  and  $\mathcal{G}$  on  $\mathcal{E}$  has been obtained by using the expressions (61) and either of the two equations (59) or (60). An illustration of

the conductance  $\mathcal{G}$  ( $= \mathcal{G}_{B \leftarrow A} = \mathcal{G}_{B \rightarrow A}$ ) for each value of the energy  $\mathcal{E}$  is provided in Figure 14a for  $N = 6$  and in Figure 14b for  $N = 10$ . The energy band curves (for incident even modes) are shown as black curves on the left side of Figures 14a and 14b. Incidentally, the same in Figure 14a are obtained by superimposing the energy bands in Figures 12a and 12b. The ballistic limit  $\mathcal{G}^{\text{ball}}$  (maximum conductance) is shown in red color while the shaded orange region represents the reduction in the conductance due to the scattering effect of the junction. Observe that the conductance  $\mathcal{G}$  near the Dirac points coincides with the

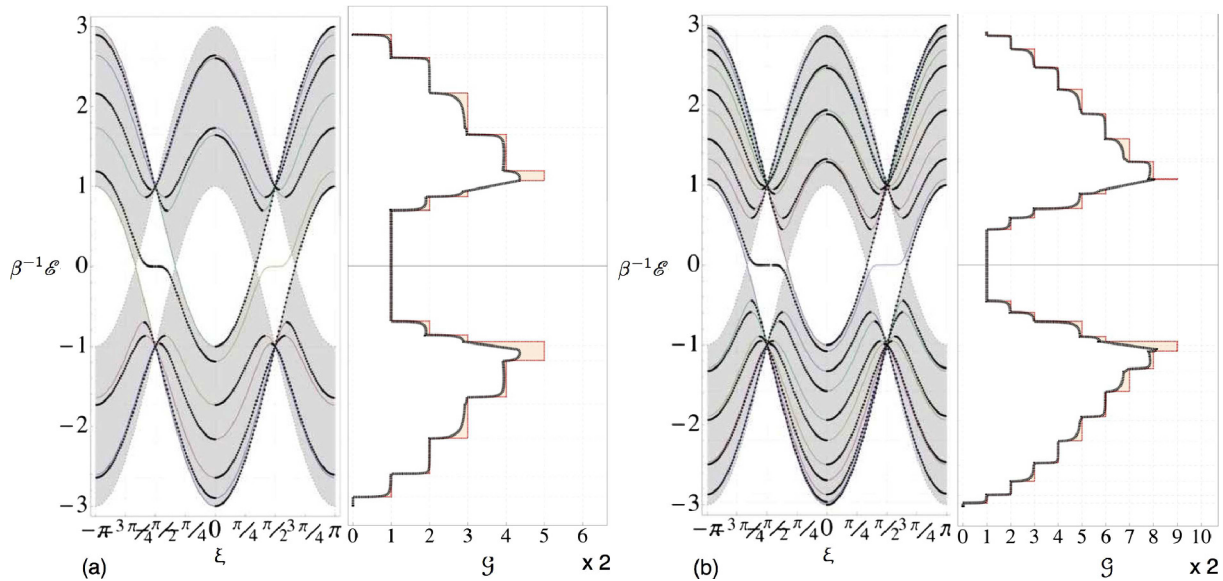


**Fig. 14.** Conductance  $\mathcal{G}$  for (a)  $N = 6$  and (b)  $N = 10$ . Also shown are the energy bands for even modes, the dark curves represent the incident wave modes (positive slope for incidence from tubular part and negative slope for ribbon) while curves in lighter shade are the transmitted/reflected counterparts.

ballistic limit  $\mathcal{G}^{\text{ball}}$ . Also the maximum departure of the conductance  $\mathcal{G}$  away from the ballistic limit  $\mathcal{G}^{\text{ball}}$  appears to be located slightly below and above the Dirac cones. If the Fermi level lies in this region then the structural properties and related details of the interaction/hopping can influence the amount of deviation.

## 8 Discussion and conclusion

The role of defects and boundaries in the context of thermoelectric power [73] is a technologically relevant issue at present. The paper presents an analysis of the propagating modes of electronic waves across a junction of semi-infinite nanoribbon and nanotube. Thus, the energy bands and the wave modes in the two leads interact via the junction and transform according to the well established scattering matrix framework. In fact, as a rather surprising find, it is observed that the expressions of the reflectance  $\mathcal{R}$  and transmittance  $\mathcal{T}$  (recall (57) and (58)) are same as those stated by [62] for bifurcated waveguides of square lattice. In other words, the formula for conductance of the  $(N - 1)$ -zigzag nanoribbon/ $(N, N)$ -armchair nanotube junction coincides with that for the bifurcated square lattice waveguides except for the expression of the kernel in the Wiener–Hopf formulation due to differences associated with honeycomb structure of the leads vs. the square lattice. Since the kernel is related to the Green’s function for the lattice structures, this is not surprising in view of the existing framework for conductance based on the Green’s function [40,70]. The analytical flavor provided in the present paper to the available computational results [27,30,65] is reckoned a constructive addition towards the physics of ballistic conduction across nanojunctions.

With respect to the past researches, using Figures 12 and 14, it is easy to see that the property of perfect

valley filtering for CNTs, at certain energy range, persists, thus continuing the related conclusion and observations of [27]. A statement concerning the electron–electron interactions, via a possible inclusion of Hubbard term, as well as the behavior of magnetoresistance using the Zeeman coupling (after incorporating the electron spin in the model) requires further analysis using computational tools as it appears to fall outside the limits of analytically solvable model.

In contrast to the partial unzipping of armchair nanotubes [27,30,65], the case of the structure studied in the present manuscript can be described as the one with an additional “defect”. From a structural viewpoint, it can be also described in terms of the existence of “double” crack (vs. “single” zigzag crack in case of partially unzipped armchair nanotubes). A careful look at the contours of the scattered wave function shown in Figures 6a–11a reveals a signature of the asymmetry with respect to the edge where the unzipped portion begins. In fact, the “asymmetric defect” leads to a mixing of symmetric modes (even and odd symmetries as prescribed by [50]) which does not happen in the case of partially unzipped armchair nanotubes due to the presence of symmetry (within the nearest-neighbor tight binding approximation which has been also used for these problems [27]). The latter has some features similar to the case of kinematically restricted phonons as analyzed in [31] with the additional feature that even modes are also scattered. An (exact solution based) analysis similar to that presented in this paper as well as [31] is anticipated to bring out the analytical flavor for the case of electronic transmission across a “single” zigzag crack (partially unzipped armchair nanotubes); the details will be presented elsewhere. Figure 15 depicts the visual relationship between even/even, even/odd, odd/even, odd/odd energy bands for incident/reflected wave modes for both directions of incidence, while emphasising at the same

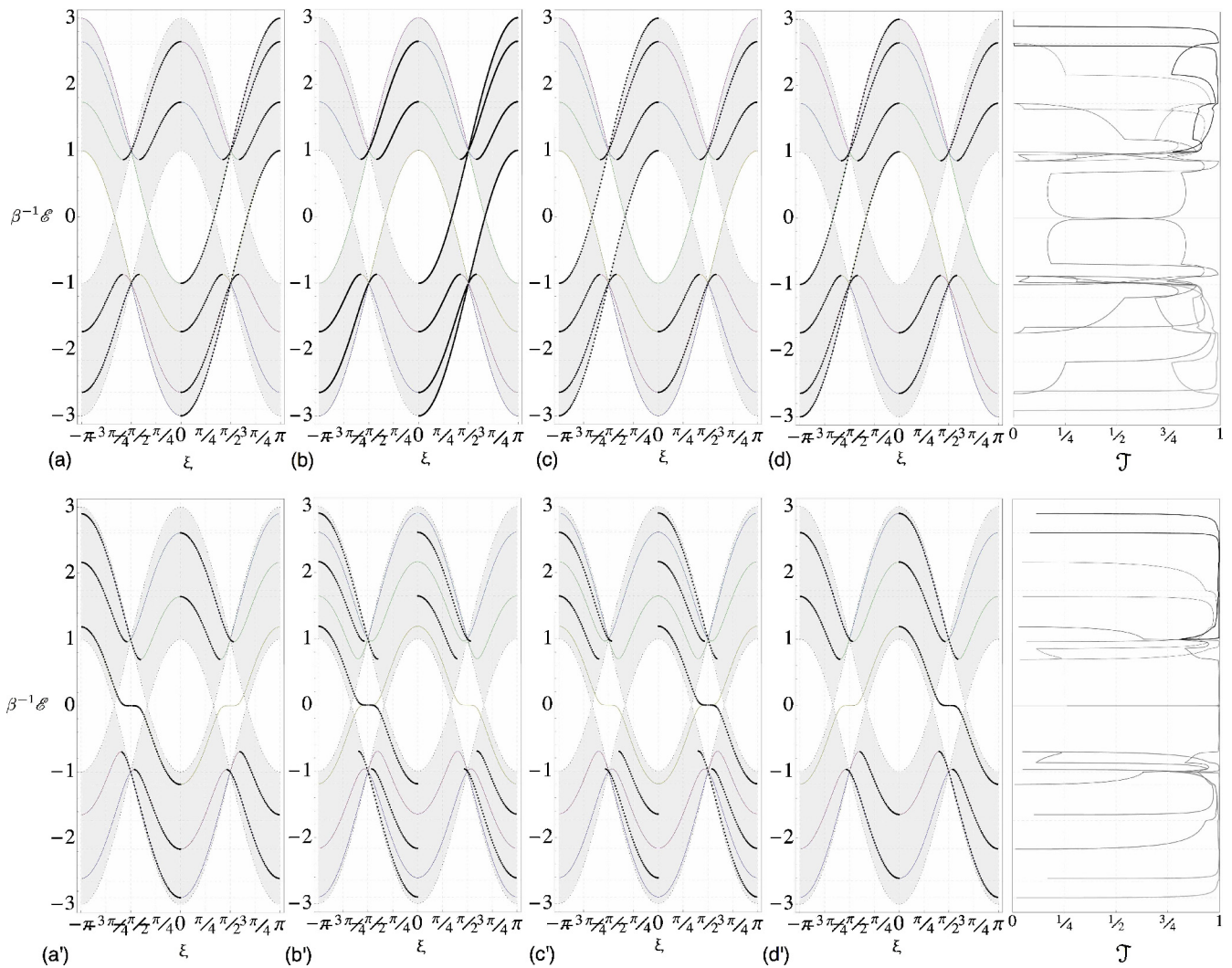


**Fig. 15.** Energy bands corresponding to the incidence (in black color) of an even (resp. odd) mode and reflected modes (in other colors) in the tubular portion of (a) (resp. (c)) even and (b) (resp. (d)) odd symmetry. Energy bands corresponding to the incidence (in black color) of an even (resp. odd) mode and reflected modes in the ribbon portion of (a) (resp. (c)) even and (b) (resp. (d)) odd symmetry. The extreme left plots show the common graph of transmittance into the other portion of the junction (note that  $\mathcal{R} = 1 - \mathcal{T}$ ) which is same as that of Figure 12.

time that the transmittance and reflection between all such combinations of parities remains the same.

Despite its well founded character from a historical point of view of the electronic states of graphene, there are several limitations of the analysis presented in the paper. For example,

- The effects of curvature on the nanotube side are neglected while the effects of the perturbations (lattice spacing, hopping interactions, dangling bonds, hydrogen-saturation, etc.) at boundary sites on the nanoribbon side are neglected [65].
- The current at Fermi level is altered by the exact shape of the energy band (see the middle curve in the left side of both plots in Fig. 14, for example) close to it; the detailed information of the electronic interactions as well as edge properties affect the same; as a related example, a gap is open close to Fermi

energy [27,30]. Detailed investigation on the lines of [65] may reveal more physical effects.

- The scattering due to bulk impurities/defects is neglected inside the leads, which is indispensable for a more realistic view of the junction.
- A complete analysis of electronic transport involving the thermal effect and electron–phonon interaction has not been done.
- Last but not the least, note that the electron–electron interactions have been neglected in the assumed highly simplified TB approximation [35]. Experimental evidence for Luttinger liquid behavior in CNTs has been pointed out by one of the reviewers, suggesting that this is more serious approximation [74,75] than those listed above.

The relevance of the provided results for a complicated arrangement of scatterers is implicit. Although the double

junction structures are not analyzed in this paper due to their strong numerical flavor (see for example [53] for a pair of edges in infinite lattice), the analysis of this paper can be extended using the existing framework of scattering matrices for dealing with a combination of scatterers. A suitable global scattering matrix can be obtained by the composition of the individual scattering matrices associated with each scatterer/interface. For example, such scattering matrix based approach for treating the electron wave propagation in complicated geometries has been illustrated, along with its advantages, by [52].

The relation between the present derivation with the more common Green's function based approach [40] is out of scope of this paper. The closed form expression provided in the paper can be considered as a reference model and perturbations around it can be studied in order to capture the realistic case using several analytical/numerical tools [27,76,77]. The analysis of the partly unzipped armchair nanotube [27,30] for non-interacting electrons is possible based on the approach followed in this paper and [31], this will be presented in future elsewhere.

The author thanks N. Sinha for reading the manuscript. The partial support of IITK/ME/20090027 is gratefully acknowledged. The author thanks the anonymous reviewers for several constructive comments and suggestions.

## Appendix A: General solution in nanotube

The discrete Fourier transform defined by

$$\psi_y^F = \psi_{y,+} + \psi_{y,-}, \text{ where}$$

$$\psi_{y,+}(z) = \sum_{x=0}^{+\infty} \psi_{x,y} z^{-x}, \quad \psi_{y,-}(z) = \sum_{x=-\infty}^{-1} \psi_{x,y} z^{-x}. \quad (\text{A.1})$$

for any fixed  $y \in \mathbb{Z}$  corresponding to the lattice structure, is analytic inside an annulus in  $\mathbb{C}$ , defined by (analogous to the statement in Appendix A of [62], in particular Eq. (A.1))

$$\mathcal{A}_\psi := \{z \in \mathbb{C} : R_+ < |z| < R_-\},$$

$$R_+ = e^{-\kappa_2}, \quad R_- = e^{+\kappa_2}. \quad (\text{A.2})$$

Using the discrete Fourier transform (A.1), away from the defect sites,

$$Q \psi_y^F - (\psi_{y+1}^F + \psi_{y-1}^F) = 0,$$

where  $Q = -\Upsilon^{-1}(\beta^{-1}\mathcal{E} - 1)(\beta^{-1}\mathcal{E} + 1) + \Upsilon$  on  $\mathbb{C}$ .

$$(\text{A.3})$$

The above equations (A.1)–(A.3) continue to hold for  $\psi^*$  using  $\mathbf{x}^*, \mathbf{y}^*$  (in place of  $\mathbf{x}, \mathbf{y}$ ). The function  $\lambda$  is defined by (appearing in several discrete scattering problems

[42,53,54,58,78,79])

$$\lambda := \frac{r - \mathfrak{h}}{r + \mathfrak{h}} \text{ on } \mathbb{C} \setminus \mathcal{B},$$

$$\text{where } \mathfrak{h} := \sqrt{\mathcal{H}}, \quad r := \sqrt{\mathcal{R}}, \quad \mathcal{R} := Q + 2, \quad \mathcal{H} := Q - 2. \quad (\text{A.4})$$

Let

$$\mathcal{M} = -\beta^{-1}\mathcal{E}^{-1}(1 - \lambda\Upsilon),$$

$$\mathcal{X} = -\beta^{-1}\mathcal{E}^{-1}(1 - \lambda^{-1}\Upsilon). \quad (\text{A.5})$$

Also  $(\beta^{-1}\mathcal{E})^2 - 1 = \Upsilon^2 - \Upsilon Q$ , which yields [42,53]  $\mathcal{X}\mathcal{M} = 1$ , and  $(1 + \lambda\mathcal{M}) = \mathcal{P}\lambda(1 + \lambda^{-1}\mathcal{M})$ .

Recall that (Footnote 4) that the periodic boundary conditions are possible (in armchair nanotube) only when  $N$  is an even number. Let  $\psi_{\mathbf{y}^*}^{*F} = C_1 \lambda^{\mathbf{y}^*} + C_2 \lambda^{-\mathbf{y}^*}$ ,  $\mathbf{y}^* \in \mathbb{Z}_0^{N-1}$ , which implies  $\psi_{\mathbf{y}}^F = \mathcal{M} C_1 \lambda^{\mathbf{y}-1} + \mathcal{X} C_2 \lambda^{-\mathbf{y}+1}$ ,  $\mathbf{y} \in \mathbb{Z}_1^N$ , and, due to the manufactured symmetry,  $\psi_{-\mathbf{y}}^F = \psi_{\mathbf{y}}^{*F}$ ,  $\mathbf{y} \geq 0$ . So  $\psi_{-\mathbf{y}}^F = C_1 \lambda^{\mathbf{y}} + C_2 \lambda^{-\mathbf{y}}$ ,  $\mathbf{y} \in \mathbb{Z}_0^{N-1}$ , and also,  $\psi_{-\mathbf{y}^*}^{*F} = \mathcal{M} C_1 \lambda^{\mathbf{y}^*-1} + \mathcal{X} C_2 \lambda^{-\mathbf{y}^*+1}$ ,  $\mathbf{y}^* \in \mathbb{Z}_1^N$ . Due to the periodicity, it is required that  $\psi_N^F = \psi_{-N}^F$ ; or  $\psi_N^{*F} = \psi_{-N}^{*F}$ . Thus,  $C_1 + C_2 = \psi_0^F = \psi_0^{*F}$ , and also  $(\mathcal{M} - \lambda)\lambda^{N-1} C_1 + (\mathcal{X} - \lambda^{-1})\lambda^{-N+1} C_2 = 0$ . Solving for  $C_1$  and  $C_2$  using both equations, with

$$\Lambda_{\mathbf{y}^*}^* = \frac{((\mathcal{X} - \lambda^{-1})\lambda^{-n+1})\lambda^{\mathbf{y}^*} - ((\mathcal{M} - \lambda)\lambda^{n-1})\lambda^{-\mathbf{y}^*}}{(\mathcal{X} - \lambda^{-1})\lambda^{-n+1} - (\mathcal{M} - \lambda)\lambda^{n-1}}, \quad (\text{A.6})$$

for periodic boundary condition

$$\psi_{\mathbf{y}^*}^{*F} = \psi_0^{*F} \Lambda_{\mathbf{y}^*}^* \text{ for } \mathbf{y}^* \in \mathbb{Z}_0^{N-1}, \quad (\text{A.7a})$$

$$\psi_{\mathbf{y}}^F = \psi_{-\mathbf{y}}^{*F} \text{ for } \mathbf{y} \in \mathbb{Z}_{-N+1}^0. \quad (\text{A.7b})$$

In particular,

$$\psi_1^F = C_1 \mathcal{M} + C_2 \mathcal{X} = \mathcal{M}_N \psi_0^{*F}, \quad (\text{A.8})$$

where  $\mathcal{M}_N$  is defined by (15).

## Appendix B: Symmetric modes and normalization constants

### B.1 Chebyshev polynomials: identities

Following the Appendix 1 of [50], the Chebyshev polynomial of first kind and second kind is  $T_n(\vartheta) = \frac{1}{2}((\vartheta + \sqrt{\vartheta^2 - 1})^n + (\vartheta - \sqrt{\vartheta^2 - 1})^n)$ ,  $U_n(\vartheta) = \frac{1}{2}((\vartheta + \sqrt{\vartheta^2 - 1})^n - (\vartheta - \sqrt{\vartheta^2 - 1})^n) / \sqrt{\vartheta^2 - 1}$ , respectively. Several identities involving the Chebyshev polynomials find applications in the paper, for example, [47]:

$$T_n = \frac{1}{2}(U_n - U_{n-2}), \quad U_n = 2\vartheta U_{n-1} - U_{n-2}, \quad (\text{B.1a})$$

$$U_n^2 = 1 + U_{n-1}U_{n+1}, \quad (\text{B.1b})$$

$$T'_n = n U_{n-1}, U'_n = (n+1)(\vartheta^2 - 1)^{-1} T_{n+1}. \quad (\text{B.1c})$$

## B.2 Modes in nanotube

Assuming the even reflection symmetry about the line between the lattice rows at  $\mathbf{y} = \mathbf{y}^* = 0$ , with the periodic boundary condition [50] (B2), the energy bands are given by

$$(1 - \mathcal{P}^2) U_{N-1}(\vartheta) = 0. \quad (\text{B.2})$$

The eigenvector components (with even reflection symmetry on the rectangular structure  $\mathfrak{H}^\circledast \cup \mathfrak{H}^\circledast^R$  containing the armchair nanotube  $\mathfrak{H}^\circledast$ , see Appendix B.2 of [50]) are given by<sup>7</sup>

$$\begin{aligned} a^*_{(\kappa)\nu} &= \mathbf{C}_\kappa^{-1}(\mathcal{P} \sin(\nu-1)\eta_\kappa - \sin \nu \eta_\kappa), \quad \nu \in \mathbb{Z}_1^N, \\ a_{(\kappa)\nu} &= \mathbf{C}_\kappa^{-1}(\sin(\nu-1)\eta_\kappa - \mathcal{P} \sin \nu \eta_\kappa), \quad \nu \in \mathbb{Z}_1^N. \end{aligned} \quad (\text{B.3})$$

and the normalization constant using the identities stated and derived in [80]  $\mathbf{C}_\kappa^2$  can be easily found for  $\mathcal{P}^2 \neq 1$  (as derived in (B.4)) to be  $N\beta^{-1}\mathcal{E}\Upsilon^{-1}(1 - \mathcal{P}^2)$  on armchair nanotube  $\mathfrak{H}^\circledast$ . When  $\mathcal{P}^2 = 1$ , similar analyses can be done as described below.

By (106a) and (106d) of [80], using (B.2) and the definition of  $Q$ , when  $1 - \mathcal{P}^2 \neq 0$ ,

$$\begin{aligned} \mathbf{C}_\kappa^2 &= (\mathcal{P}^2 + 1) \sum_{\nu=1}^N \sin^2 \nu \eta_\kappa + (\mathcal{P}^2 + 1) \sum_{\nu=1}^N \sin^2(\nu-1)\eta_\kappa \\ &\quad - 2\mathcal{P}(1+1) \sum_{\nu=1}^N \sin \nu \eta_\kappa \sin(\nu-1)\eta_\kappa \\ &= N(-\beta^{-1}\mathcal{E})\Upsilon^{-1}(\mathcal{P}^2 - 1). \end{aligned} \quad (\text{B.4})$$

Note that (using  $(\beta^{-1}\mathcal{E})^2 - 1 = \Upsilon^2 - \Upsilon Q$ )

$$\mathcal{P}^2 - 1 = 2\Upsilon(\mathcal{P} - \vartheta), \quad (\text{B.5})$$

so that by (B.3),

$$\begin{aligned} a^*_{(\kappa)\nu} &= \mathbf{C}_\kappa^{-1} \cos(\nu-1)\eta_\kappa, \quad \nu \in \mathbb{Z}_1^N, \\ a_{(\kappa)\nu} &= \mathbf{C}_\kappa^{-1} \cos \nu \eta_\kappa, \quad \nu \in \mathbb{Z}_1^N. \end{aligned} \quad (\text{B.6})$$

Using (B.6), when  $1 - \mathcal{P}^2 = 0$ ,

$$\begin{aligned} \mathbf{C}_\kappa^2 &= \sum_{\nu=1}^N |\cos(\nu-1)\eta_\kappa|^2 + \sum_{\nu=1}^N |\cos \nu \eta_\kappa|^2 \\ &= N + \frac{1}{2}(U_{2N} - 1) = 2N. \end{aligned} \quad (\text{B.7})$$

<sup>7</sup> With reference to Figure 3, notice that in (B.3)<sub>1</sub> (resp. (B.3)<sub>2</sub>)  $\nu$  corresponds to  $\mathbf{y}^* + 1$  (resp.  $\mathbf{y}$ ).

For above, we used  $\sin^2 \eta_\kappa = 1 - \cos^2 \eta_\kappa = 1 - \vartheta^2 = 1 - \mathcal{P}^2 = 0$ .

In the case of odd reflection symmetry, the above analysis can be repeated. Following Appendix B.2 of [50], in the presence of odd reflection symmetry about the line between the lattice rows at  $\mathbf{y} = \mathbf{y}^* = 0$ , i.e.,  $a_{-\mathbf{y}} = -a^*_{\mathbf{y}}, \mathbf{y} \in \mathbb{Z}_0^{N-1}$ . This yields the condition  $-a_{-\mathbf{y}} = C_1 \lambda^{\mathbf{y}} + C_2 \lambda^{-\mathbf{y}}, \mathbf{y} \in \mathbb{Z}_0^{N-1}$ , and also,  $-a^*_{-\mathbf{y}^*} = \mathcal{M} C_1 \lambda^{\mathbf{y}^*-1} + \mathcal{N} C_2 \lambda^{-\mathbf{y}^*+1}, \mathbf{y}^* \in \mathbb{Z}_1^N$ . Due to periodicity, it is required that  $a_N = a_{-N}$ , or, equivalently,  $a^*_N = a^*_{-N}$ . The odd reflection symmetry,  $a_0 = -a^*_0$  results in an additional equation using the discrete Helmholtz equation. The relations  $(\beta^{-1}\mathcal{E} + \Upsilon + \mathcal{M}) C_1 + (\beta^{-1}\mathcal{E} + \Upsilon + \mathcal{N}) C_2 = 0$ ,  $(\mathcal{M} + \lambda)\lambda^{N-1} C_1 + (\mathcal{N} + \lambda^{-1})\lambda^{-N+1} C_2 = 0$ , admit a nontrivial solution for  $C_1$  and  $C_2$  so that the energy bands are given by

$$(1 - \tilde{\mathcal{P}}^2) U_{N-1}(\vartheta) = 0, \quad (\text{B.8})$$

where  $\tilde{\mathcal{P}} = \beta^{-1}\mathcal{E} + \Upsilon$ . The eigenvector components (with odd reflection symmetry on rectangular structure  $\mathfrak{H}^\circledast \cup \mathfrak{H}^\circledast^R$  containing the armchair nanotube  $\mathfrak{H}^\circledast$ , see Appendix B.2 of [50]) are given by

$$\begin{aligned} a^*_{(\kappa)\nu} &= \mathbf{C}_\kappa^{-1}(\tilde{\mathcal{P}} \sin(\nu-1)\eta_\kappa - \sin \nu \eta_\kappa), \quad \nu \in \mathbb{Z}_1^N, \\ a_{(\kappa)\nu} &= \mathbf{C}_\kappa^{-1}(\sin(\nu-1)\eta_\kappa - \tilde{\mathcal{P}} \sin \nu \eta_\kappa), \quad \nu \in \mathbb{Z}_1^N, \end{aligned} \quad (\text{B.9})$$

where

$$\mathbf{C}_\kappa^2 = -N(-\beta^{-1}\mathcal{E})\Upsilon^{-1}(\tilde{\mathcal{P}}^2 - 1), \quad (\text{B.10})$$

for  $1 - \tilde{\mathcal{P}}^2 \neq 0$ . The analysis for  $1 - \tilde{\mathcal{P}}^2 = 0$  is straightforward.

## B.3 Modes in nanoribbon

Assuming the even reflection symmetry about the line midway between the lattice rows at  $\mathbf{y} = \mathbf{y}^* = 0$ , with the Dirichlet boundary condition [50] (3.20), the energy bands are given by

$$\mathcal{P} U_{N-1}(\vartheta) - U_{N-2}(\vartheta) = 0. \quad (\text{B.11})$$

The eigenmodes<sup>8</sup> (symmetric on the rectangular structure  $\mathfrak{H}^\bullet \cup \mathfrak{H}^\bullet^R$  containing  $\mathfrak{H}^\bullet$ ) in zigzag nanoribbon  $\mathfrak{H}^\bullet$  are given by equations (3.21) and (3.22) of [50], i.e.,<sup>9</sup>

$$\begin{aligned} a^*_{(\kappa)\nu} &= \mathbf{C}_\kappa^{-1}(\mathcal{P} \sin(\nu-1)\eta_\kappa - \sin \nu \eta_\kappa), \quad \nu \in \mathbb{Z}_1^N, \\ a_{(\kappa)\nu} &= \mathbf{C}_\kappa^{-1}(\sin(\nu-1)\eta_\kappa - \mathcal{P} \sin \nu \eta_\kappa), \quad \nu \in \mathbb{Z}_1^{N-1}. \end{aligned} \quad (\text{B.12})$$

<sup>8</sup> Alternative to (B.12), Eq. (3.8) of [50]  $a_{(\kappa)\nu} = \mathbf{C}_\kappa^{-1}(\Upsilon \sin \nu \eta_\kappa - \sin(\nu-1)\eta_\kappa)$ ,  $a^*_{(\kappa)\nu} = \mathbf{C}_\kappa^{-1} \beta^{-1}\mathcal{E} \sin \nu \eta_\kappa, \nu \in \mathbb{Z}_1^{N-1}$  (note  $N = 2N$ ). but, as it is clear, the normalization  $\mathbf{C}_\kappa$  is not the same.

<sup>9</sup> With reference to Figure 3, notice that in (B.12)<sub>1</sub> (resp. (B.12)<sub>2</sub>)  $\nu$  corresponds to  $\mathbf{y}^* + 1 - N$  (resp.  $\mathbf{y} - N$ ).

It is easy check that  $a_{(\kappa)N} = 0$  (which corresponds to the condition (B.11) on  $\eta_{\kappa}$ ). The normalization constant (using the identities stated and derived in [80]  $\mathcal{C}_{\kappa}^2$  can be easily found as described below.

By (B.12) (with reasoning similar to that for (B.4)),

$$\mathcal{C}_{\kappa}^2 = (\mathcal{P}^2 - 1)(N(-\beta^{-1}\mathcal{E})\Upsilon^{-1} + \frac{1}{2}(-\beta^{-1}\mathcal{E})^{-1}(\vartheta - \Upsilon^{-1})). \quad (\text{B.13})$$

Note that  $\mathcal{U}_{N-1}^2 = 1 + \mathcal{U}_N \mathcal{U}_{N-2} = 1 + (Q - \mathcal{P})\mathcal{P}\mathcal{U}_{N-1}^2$  so that  $(\mathcal{P}^2 + 1 - 2\vartheta\mathcal{P})\mathcal{U}_{N-1}^2 = 1$  where it can be shown that  $\mathcal{P}^2 + 1 - 2\vartheta\mathcal{P} = (\mathcal{P}^2 - 1)\Upsilon^{-1}(-\beta^{-1}\mathcal{E})$ . Also  $(2\mathcal{P} - \vartheta(\mathcal{P}^2 + 1)) = 2(\mathcal{P} - \vartheta)(1 - \Upsilon\vartheta)$  so that  $(\vartheta - \mathcal{P})(2\mathcal{P} - \vartheta(\mathcal{P}^2 + 1)) = -2(\mathcal{P} - \vartheta)^2(1 - \Upsilon\vartheta) = (\mathcal{P}^2 - 1)(\mathcal{P} - \vartheta)(\vartheta - \Upsilon^{-1})$ .

In the case of odd reflection symmetry, the above analysis can be also repeated. Following Section 3.1.2 of [50], it is found that the energy bands are given by

$$\tilde{\mathcal{P}}\mathcal{U}_{N-1}(\vartheta) - \mathcal{U}_{N-2}(\vartheta) = 0. \quad (\text{B.14})$$

The eigenmodes are

$$\begin{aligned} a^*_{(\kappa)\nu} &= \mathcal{C}_{\kappa}^{-1}(\tilde{\mathcal{P}}\sin(\nu-1)\eta_{\kappa} - \sin\nu\eta_{\kappa}), \quad \nu \in \mathbb{Z}_1^N, \\ a_{(\kappa)\nu} &= \mathcal{C}_{\kappa}^{-1}(\sin(\nu-1)\eta_{\kappa} - \tilde{\mathcal{P}}\sin\nu\eta_{\kappa}), \quad \nu \in \mathbb{Z}_1^{N-1}, \end{aligned} \quad (\text{B.15})$$

where

$$\mathcal{C}_{\kappa}^2 = -(\tilde{\mathcal{P}}^2 - 1)(N(-\beta^{-1}\mathcal{E})\Upsilon^{-1} + \frac{1}{2}(-\beta^{-1}\mathcal{E})^{-1}(\vartheta - \Upsilon^{-1})). \quad (\text{B.16})$$

#### B.4 Even and odd incident modes

Notice that the denominator  $\widehat{\mathcal{D}}$  of  $\mathcal{L}$  (in (17)) contains energy bands for the even wave modes in the tubular portion of the rectangular lattice structure [80]. On the other hand, the numerator  $\mathcal{N}$  of  $\mathcal{L}$  contains energy bands for the even wave modes in the unzipped portion albeit in the form of rectangular lattice strip [50]. This is surprising in view of the allowance of an arbitrary incident wave mode, i.e., both even and odd reflection symmetries in the either side of the junction. Since  $\mathcal{U}_n(-\vartheta) = (-1)^n\mathcal{U}_n(\vartheta)$ , and (using (16))  $\vartheta(-z) = -\vartheta(z)$ , it is easy to see that,

$$\begin{aligned} \mathcal{N}(-z) &= (1 - \mathcal{P}^2(-z))\mathcal{U}_{N-1}(\vartheta(-z)) \\ &= (1 - (-\beta^{-1}\mathcal{E} + (z + z^{-1}))^2)\mathcal{U}_{N-1}(\vartheta(-z)) \\ &= (-1)^{N-1}(1 - (-\beta^{-1}\mathcal{E} + (z + z^{-1}))^2)\mathcal{U}_{N-1}(\vartheta(z)) \\ &= (-1)^{N-1}(1 - \tilde{\mathcal{P}}^2(z))\mathcal{U}_{N-1}(\vartheta(z)), \end{aligned} \quad (\text{B.17a})$$

and

$$\begin{aligned} \widehat{\mathcal{D}}(-z) &= \mathcal{U}_{N-2}(\vartheta(-z)) - \mathcal{P}(-z)\mathcal{U}_{N-1}(\vartheta(-z)) \\ &= \mathcal{U}_{N-2}(\vartheta(-z)) - (-\beta^{-1}\mathcal{E} + (z + z^{-1}))\mathcal{U}_{N-1}(\vartheta(-z)) \\ &= (-1)^{N-1}(-\mathcal{U}_{N-2}(\vartheta(z)) - (-\beta^{-1}\mathcal{E} + (z + z^{-1}))\mathcal{U}_{N-1}(\vartheta(z))) \\ &= -(-1)^{N-1}(\mathcal{U}_{N-2}(\vartheta(z)) - \tilde{\mathcal{P}}(z)\mathcal{U}_{N-1}(\vartheta(z))), \end{aligned} \quad (\text{B.17b})$$

so that the corresponding expressions are precisely the energy bands for the *odd* wave modes in the tubular and unzipped portions (of the rectangular lattice structure) (B.8) and (B.14), respectively. Thus, according to (31), it is useful to define  $\mathcal{N}_o = (1 - \tilde{\mathcal{P}}^2)\mathcal{U}_{N-1}$  and  $\widehat{\mathcal{D}}_o := -(\mathcal{U}_{N-2} - \tilde{\mathcal{P}}\mathcal{U}_{N-1})$ .

### Appendix C: Wiener–Hopf procedure

The kernel  $\mathcal{L}$  (14b) can be expressed as a ratio of a polynomial  $\mathcal{N}$  (of  $z$ ) in the numerator and another polynomial  $\mathcal{D}$  (of  $z$ ) in the denominator. In fact, these can be expressed in terms of Chebyshev polynomials (see (17)) and thus, the Wiener–Hopf factors can be written down explicitly. For this purpose, [41,81] a notational device developed by [62] is employed. Let

$$F(z; z_F) := z_F^{-1}(1 - z_F z)(1 - z_F z^{-1}), \quad (\text{C.1a})$$

$$F_{\pm}(z; z_F) = z_F^{-\frac{1}{2}}(1 - z_F z^{\mp 1}). \quad (\text{C.1b})$$

Thus  $\mathcal{L}(z) = \mathcal{N}(z)/\mathcal{D}(z)$ , where

$$\mathcal{N}(z) = \prod_{j=1}^N F(z; z_{F_{N_j}}) = \mathcal{N}_+(z)\mathcal{N}_-(z), \quad (\text{C.2a})$$

$$\mathcal{D}(z) = \prod_{j=1}^N F(z; z_{F_{D_j}}) = \mathcal{D}_+(z)\mathcal{D}_-(z). \quad (\text{C.2b})$$

As  $N = 2N$ , a factor of two appears in the product limits because (16) involves  $z^2$  and  $z^{-2}$  (in place of  $z$  and  $z^{-1}$  in square lattice waveguide [62]). Indeed, it follows from (C.1b) that the Wiener–Hopf factors of  $\mathcal{N}$  and  $\mathcal{D}$  are, respectively, given by

$$\begin{aligned} \mathcal{N}_{\pm}(z) &= \prod_{j=1}^N F_{\pm}(z; z_{F_{N_j}}), \\ \mathcal{D}_{\pm}(z) &= \prod_{j=1}^N F_{\pm}(z; z_{F_{D_j}}). \end{aligned} \quad (\text{C.3})$$

The factors  $\mathcal{L}_\pm$  are, therefore, given by

$$\mathcal{L}_\pm(z) = \frac{\mathcal{N}_\pm(z)}{\mathcal{D}_\pm(z)} = \frac{\prod_{j=1}^N F_\pm(z; z_{F_{N_j}})}{\prod_{j=1}^N F_\pm(z; z_{F_{D_j}})}. \quad (\text{C.4})$$

In view of the above definitions, let

$$R_L := \max(\{|z_{F_{N_j}}|\}_{j=1}^N \cup \{|z_{F_{D_j}}|\}_{j=1}^N), \quad (\text{C.5a})$$

$$\mathcal{A}_L := \{z \in \mathbb{C} : R_L < |z| < R_L^{-1}\}. \quad (\text{C.5b})$$

With  $\mathcal{L}_\pm = \mathcal{N}_\pm/\mathcal{D}_\pm$ , the multiplicative factorization [41] of  $\mathcal{L}$  in (14b) is given by

$$\mathcal{L}(z) = \mathcal{L}_+(z)\mathcal{L}_-(z), \quad z \in \mathcal{A}_L. \quad (\text{C.6})$$

Note that the complex function  $\mathcal{L}_+$  (resp.  $\mathcal{L}_-$ ) is analytic, without any zeros, in the exterior (resp. interior) of a disk centered at 0 in  $\mathbb{C}$  with radius  $R_L$  (resp.  $R_L^{-1}$ ). This means that  $1/\mathcal{L}_+$  (resp.  $1/\mathcal{L}_-$ ) is analytic in the same region as  $\mathcal{L}_+$  (resp.  $\mathcal{L}_-$ ). The property  $\mathcal{L}_\pm(z) = \mathcal{L}_\mp(z^{-1})$  aids to obtain a unique factorization [41]. Let  $\mathcal{A}$  be an annulus defined by

$$\mathcal{A} := \mathcal{A}_\psi \cap \mathcal{A}_L, \quad (\text{C.7})$$

with  $\mathcal{A}_\psi$  given by (A.2). Substituting (C.6) in (14a), after rearrangement, it is found that

$$\mathcal{L}_+\psi_{1,+} + \mathcal{L}_-^{-1}\psi_{1,-} = C \text{ on } \mathcal{A}, \quad (\text{C.8})$$

$$\text{where } C = (\mathcal{W} + \mathcal{P}\psi_{0,-}\delta_{\mathbf{s},\mathbf{A}} + \psi_{1,+}^i\delta_{\mathbf{s},\mathbf{B}}) \times (\mathcal{L}_-^{-1} - \mathcal{L}_+). \quad (\text{C.9})$$

The function  $\delta_{D^\mp}(zz_P^{-1})$  is analytic at all  $z$  in  $\mathcal{A}$  (C.7), and its only singularity is a simple pole at  $z = z_P$ , which lies outside (resp. inside) the annulus  $\mathcal{A}$ . Substituting (10d), (10c), and (10b) in (C.9), the additive factorization  $C = C_+ + C_-$  is constructed yielding (using the symmetry of modes on the rectangular lattice structure),

$$\begin{aligned} C_\pm(z) &= \pm\psi_{-1,0}^i(\mathcal{L}_\pm^{\pm 1}(z) - \bar{l}_{-0}) \\ &\quad \pm z\psi_{0,0}(\mathcal{L}_\pm^{\pm 1}(z) - l_{+0}) \\ &\quad \pm Aa^i(z_P^{-1}\bar{l}_{-0} - zl_{+0})\delta_{\mathbf{s},\mathbf{A}} \\ &\quad \pm Aa^i \frac{-z}{z - z_P}(\mathcal{L}_\pm^{\pm 1}(z)\mathcal{P}(z) - \mathcal{L}_+(z_P)\mathcal{P}(z_P))\delta_{\mathbf{s},\mathbf{A}} \\ &\quad \pm Aa^i \frac{-z}{z - z_P}(\mathcal{L}_\pm^{\pm 1}(z) - \mathcal{L}_-^{-1}(z_P))\delta_{\mathbf{s},\mathbf{B}}, \end{aligned} \quad (\text{C.10})$$

where  $l_{\pm 0} = \lim_{z \rightarrow \infty} \mathcal{L}_\pm(z^{\pm 1})$ .

The function  $C_+(z)$  (resp.  $C_-(z)$ ) is analytic at  $z \in \mathbb{C}$  such that  $|z| > \max\{R_+, R_L\}$  (resp.  $|z| < \min\{R_-, R_L^{-1}\}$ ).

Upon substitution of (C.10) in (C.8), after rearrangement, define

$$\begin{aligned} J(z) &:= \mathcal{L}_+(z)\psi_{1,+}(z) - C_+(z) \\ &= -\frac{\psi_{1,-}(z)}{\mathcal{L}_-(z)} + C_-(z), \end{aligned} \quad (\text{C.11})$$

for  $z \in \mathcal{A}$ . The function  $J(z)$  is analytic at  $z \in \mathbb{C}$  with  $|z| > \max\{R_+, R_L\}$ , and also at  $z \in \mathbb{C}$  with  $|z| < \min\{R_-, R_L^{-1}\}$ , i.e., it is entire. Using (C.6), (A.1), and (C.10), as  $z \rightarrow 0$ ,  $\mathcal{L}_-(z) \rightarrow C_1$ ,  $\psi_-(z) \rightarrow 0$ , and  $C_-(z) \rightarrow 0$ , while as  $z \rightarrow \infty$ ,  $\mathcal{L}_+(z) \rightarrow C_2$ ,  $\psi_+(z) \rightarrow C_3$  and  $C_+(z) \rightarrow C_4$ , hence, it follows that  $J(z)$  is bounded on the complex plane and tends to zero as  $z$  tends to 0. By Liouville's theorem [59],  $J$  vanishes everywhere.

## Appendix D: Numerical scheme

The discrete Helmholtz equation, and the boundary conditions, are algebraic so that the numerical solution on a  $(2N_{\text{grid}} + 1) \times N$  grid  $\Omega$  can be obtained by employing on the left and right edges of  $\Omega$ , a variant [82] of perfectly matched layers (PML) [83] for simulation of an ‘‘infinite’’ strip. Introducing  $\sigma_{x,y} = \frac{1}{N_{\text{grid}}}H(|\mathbf{x}| - N_{\text{pml}})|N_{\text{pml}} - |\mathbf{x}||$ , the discrete Helmholtz equation in intact lattice is replaced by (with the same equation for starred sites modulo the replacement of  $\psi$  by  $\psi^*$ )

$$\Delta\psi_{x,y} + \frac{3}{2}\omega_{\text{H}}^2 \left(1 - \frac{\sigma_{x,y}}{i\omega_{\text{H}}^2}\right)^2 \psi_{x,y} = 0, \quad (\mathbf{x}, \mathbf{y}) \in \Omega \setminus \Sigma, \quad (\text{D.1})$$

where

$$\omega_{\text{H}}^2 = 6 \left(1 + \frac{1}{3}\beta^{-1}\mathcal{E}\right) \left(1 - \frac{1}{3}\beta^{-1}\mathcal{E}\right). \quad (\text{D.2})$$

This provides a left and right absorbing layer that has been used in the numerical computations.

The relation (Fig. D.1) between slant coordinates  $(m, n)$  and alternate coordinates  $(m_a, n_a)$  for the honeycomb lattice is quite handy for the numerical calculations. The physical honeycomb lattice  $\mathfrak{H}$  requires  $m_a = m + \frac{1}{2}(n \bmod (n, 2))$ ,  $n_a = n$ . So for these sites  $\mathbf{x} = 2m + n = 2m_a + \bmod(n_a, 2)$ ,  $\mathbf{y} = n = n_a$ .

## Appendix E: Simplification of reflection and transmission moduli

### E.1 Reflection

In order to simplify (50), consider  $\vartheta \equiv \vartheta(z, \mathcal{E})$ , i.e.,  $\vartheta$  as a function of  $z$  and  $\mathcal{E}$ ; the same consideration applies to other relevant functions.<sup>10</sup> Thus,  $\mathcal{D}(z, \mathcal{E}) = 0$  provides an

<sup>10</sup> Suppose that  $'$ , with exception to the  $'$  with Chebyshev polynomials where it refers to the derivative with respect to the argument  $\vartheta$ , refers to the derivative with respect to  $z$  while  $^\circ$  denotes the derivative  $\mathcal{E}$ .

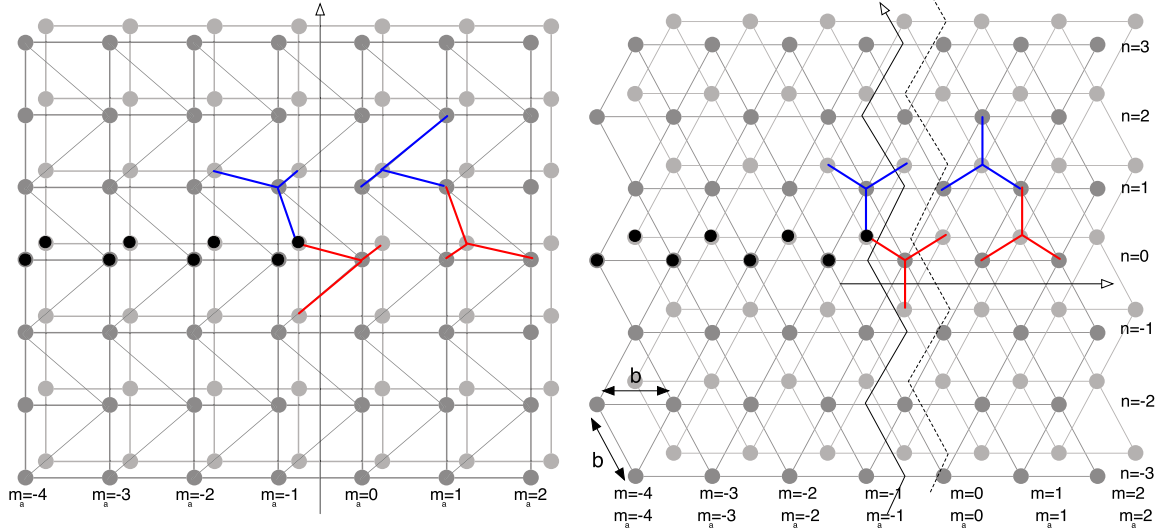


**Fig. D.1.** Numerical grid for honeycomb lattice  $\mathfrak{H}$  with a semi-infinite Dirichlet condition at  $y = 0$  and all  $x \in \mathbb{Z}$  with  $x < 0$ .

implicit definition of the energy bands  $\mathcal{E} = \mathcal{E}(\xi)$  in the ribbon portion (since  $\mathcal{D}(e^{-i\xi}, \Omega(\xi)) = 0$ ) and

$$\begin{aligned} 0 &= \frac{d}{d\xi} \mathcal{D}(z, \mathcal{E})|_{e^{-i\xi}=z, \mathcal{E}=\mathcal{E}(\xi)} \\ &= -iz \mathcal{D}'(z, \mathcal{E})|_{z=e^{-i\xi}} + \hbar v(\xi, \mathcal{E}) \widehat{\mathcal{D}}(z, \mathcal{E})|_{z=e^{-i\xi}}. \end{aligned}$$

Similarly, with  $\mathcal{N}(e^{-i\xi}, \Omega(\xi)) = 0$  (corresponding to the energy bands in the tubular portion),

$$\begin{aligned} 0 &= \frac{d}{d\xi} \mathcal{N}(z, \mathcal{E})|_{e^{-i\xi}=z, \mathcal{E}=\mathcal{E}(\xi)} \\ &= -iz \mathcal{N}'(z, \mathcal{E})|_{z=e^{-i\xi}} + \hbar v(\xi, \mathcal{E}) \dot{\mathcal{N}}(z, \mathcal{E})|_{z=e^{-i\xi}}. \end{aligned}$$

Consider that case first (recall (17)) when  $\mathcal{N} = 0$ . Assume that  $\mathcal{U}_{N-1} = 0$  (for illustrative purpose the vanishing of the other factor of  $\mathcal{N}$  (17) is omitted), then  $\mathcal{N}' = (1 - \mathcal{P}^2) \mathcal{U}'_{N-1} \vartheta' = \mathcal{N}(1 - \mathcal{P}^2) \mathcal{T}_N \vartheta' / (\vartheta^2 - 1) = \mathcal{N}(1 - \mathcal{P}^2) \mathcal{U}_N \vartheta' / (\vartheta^2 - 1)$ . This is relevant for the reflection coefficient for the incident wave from the tubular side and also for the transmission coefficient for the incidence from ribbon. Then by (E.1),

$$\begin{aligned} \hbar v(\xi, \mathcal{E}) &= \frac{iz \mathcal{N}'(z, \mathcal{E})}{\dot{\mathcal{N}}(z, \mathcal{E})} = \frac{iz \vartheta'(z, \mathcal{E})}{\dot{\vartheta}(z, \mathcal{E})} \\ &= - \left( 1 - \frac{\vartheta(z, \mathcal{E})}{\Upsilon(z)} \right) \frac{iz \Upsilon(z, \mathcal{E}) \Upsilon'(z, \mathcal{E})}{\beta^{-1} \mathcal{E} \beta^{-1}}. \end{aligned} \quad (\text{E.1})$$

Further, differentiating (16) (recall Footnote 10), it is easy to see that

$$\begin{aligned} 2\vartheta' &= (((\beta^{-1} \mathcal{E})^2 - 1) \Upsilon^{-2} + 1) \Upsilon' \\ &= 2 \Upsilon^{-1} (\Upsilon - \vartheta) \Upsilon', \end{aligned} \quad (\text{E.2})$$

$$2\dot{\vartheta} = -2\beta^{-1} \mathcal{E} \beta^{-1} \Upsilon^{-1}. \quad (\text{E.3})$$

By (16),  $\overline{\vartheta(z_a, \mathcal{E})} = \vartheta(z_a, \mathcal{E})$  and using (E.2), which implies  $\vartheta'(z_a, \mathcal{E}) / \vartheta'(z_a, \mathcal{E}) = \Upsilon'(z_a) / \Upsilon'(z_a)$ , and (E.3),

$$\frac{\hbar v}{\mathcal{N}'(z)} = \frac{(\vartheta^2 - 1) \Upsilon}{\mathcal{N}(1 - \mathcal{P}^2) \mathcal{U}_N} \frac{iz^{-1}}{\beta^{-1} \mathcal{E} \beta^{-1}}, \quad (\text{E.4})$$

so that

$$(-z z_P) \frac{\widehat{\mathcal{D}}(z) \hbar v}{\mathcal{N}'(z)} = iz_P \frac{(\vartheta^2 - 1) \Upsilon}{\mathcal{N}(1 - \mathcal{P}^2) \beta^{-1} \mathcal{E} \beta^{-1}}, \quad (\text{E.5})$$

and, eventually,

$$\begin{aligned} \frac{|a^*(\kappa^i)_1|^2}{|a^*(\kappa_z)_1|^2} (-z z_P) \frac{\widehat{\mathcal{D}}(z) \hbar v}{\mathcal{N}'(z)} &= iz_P \frac{(\vartheta^2(z_P) - 1)}{\mathcal{N} \beta^{-1} \mathcal{E} \beta^{-1}} \\ &\times \frac{1}{(1 - \mathcal{P}^2(z_P, \mathcal{E})) \Upsilon^{-1}(z_P)}. \end{aligned} \quad (\text{E.6})$$

Note that at  $z = z_P$ , it is easy to find that

$$\begin{aligned} (-z_P^2) \frac{\widehat{\mathcal{D}}(z_P, \mathcal{E}) \hbar v(z_P, \mathcal{E})}{\mathcal{N}'(z_P, \mathcal{E})} \\ = iz_P \frac{(\vartheta^2(z_P, \mathcal{E}) - 1) \Upsilon(z_P)}{\mathcal{N}(1 - \mathcal{P}^2(z_P, \mathcal{E}))} \frac{1}{\beta^{-1} \mathcal{E} \beta^{-1}}, \end{aligned} \quad (\text{E.7})$$

In the context of (50), the simplified form is

$$|\tau_{a\bar{a}}^{\text{A}\bar{\text{A}}}|^2 = \frac{1}{2} \widehat{\mathcal{C}}_a \frac{z_{\bar{a}}}{(z_a - z_{\bar{a}})^2} \frac{\overline{\mathcal{N}_-(z_a) \widehat{\mathcal{D}}_+(z_a)}}{\widehat{\mathcal{D}}_-(z_a) \mathcal{N}'_+(z_a)}, \quad (\text{E.8})$$

where  $\widehat{C}_a$  is given by (52). Recall that for above expression, it was assumed that  $(1 - \mathcal{P}^2(z_a, \mathcal{E})) \neq 0, \mathbf{U}_{N-1}(\vartheta(z_a, \mathcal{E})) = 0$  as well as  $(1 - \mathcal{P}^2(z_a, \mathcal{E})) \neq 0, \mathbf{U}_{N-1}(\vartheta(z_a, \mathcal{E})) = 0$ . Interestingly, though the detailed derivation is omitted, the same relation holds for the cases when (i)  $(1 - \mathcal{P}^2(z_a, \mathcal{E})) = 0, \mathbf{U}_{N-1}(\vartheta(z_a, \mathcal{E})) = 0$ , (ii)  $(1 - \mathcal{P}^2(z_a, \mathcal{E})) = 0, \mathbf{U}_{N-1}(\vartheta(z_a, \mathcal{E})) = 0$ , and also for the case when (iii)  $(1 - \mathcal{P}^2(z_a, \mathcal{E})) = 0, \mathbf{U}_{N-1}(\vartheta(z_a, \mathcal{E})) = 0$  for the wave incidence and reflection in the tubular side. Hence, for all  $a$  and  $\bar{a}$ , it is found that (51) holds with (52).

### E.2 Transmission

Consider the case for the transmission coefficient now. Using (38)<sub>2</sub>,

$$\begin{aligned} |\tau_{b\bar{a}}^{B\bar{A}}|^2 &= \frac{v(\xi_b)}{v(\xi_a)} \mathcal{J}_{\bar{a}b}^{\bar{A}A} \overline{\mathcal{J}_{\bar{a}b}^{\bar{A}A}} \\ &= \frac{1 - v(\xi)}{2 - v(\xi_P)} \left| \frac{\widehat{\mathcal{D}}_+(z_P)}{\mathcal{N}_+(z_P)} \right|^2 \frac{|a^*(\kappa^i)_1|^2}{|a^*(\kappa_z)_N|^2} \\ &\quad \times \left| \frac{\mathcal{N}_+(z)}{\widehat{\mathcal{D}}'_+(z)} \right|^2 \left| \frac{1}{z - z_P} \right|^2. \end{aligned} \tag{E.9}$$

Recall (17), then  $\mathcal{D} = 0$ . Consider only  $\widehat{\mathcal{D}} = \mathbf{U}_{N-2} - \mathcal{P} \mathbf{U}_{N-1} = 0$  (this gives  $\mathbf{U}_{N-2} = \mathcal{P} \mathbf{U}_{N-1}$ ,  $\mathbf{U}_N = (Q - \mathcal{P}) \mathbf{U}_{N-1}$ ,  $2 \mathbf{T}_N = (Q - 2\mathcal{P}) \mathbf{U}_{N-1}$ ,  $2 \mathbf{T}_{N-1} = (2 - Q\mathcal{P}) \mathbf{U}_{N-1}$ ) so that

$$\begin{aligned} \widehat{\mathcal{D}}' &= \mathbf{U}'_{N-2} \vartheta' - \mathcal{P} \mathbf{U}'_{N-1} \vartheta' - \mathcal{P}' \mathbf{U}_{N-1} \\ &= (N - 1) \mathbf{T}_{N-1} \frac{\vartheta'}{(\vartheta^2 - 1)} \\ &\quad - \mathcal{P} \mathbf{N} \mathbf{T}_N \frac{\vartheta'}{(\vartheta^2 - 1)} - \Upsilon' \mathbf{U}_{N-1} \\ &= \left( ((\mathcal{P}^2 + 1 - 2\mathcal{P}\vartheta)N - (1 - \vartheta\mathcal{P})) \frac{\vartheta'}{(\vartheta^2 - 1)} - \Upsilon' \right) \mathbf{U}_{N-1}. \end{aligned} \tag{E.10}$$

By (B.5),

$$\begin{aligned} \widehat{\mathcal{D}}' &= \left( (-2\beta^{-1}\mathcal{E}(\mathcal{P} - \vartheta)N - (1 - \vartheta\mathcal{P})) \frac{\Upsilon^{-1}(\Upsilon - \vartheta)}{(\vartheta^2 - 1)} - 1 \right) \\ &\quad \times \Upsilon' \mathbf{U}_{N-1} \\ &= \left( \frac{N}{\mathbf{U}_{N-1}^2} + \frac{1}{2} \frac{\Upsilon^{-1}(\mathcal{P} - \vartheta)(-\beta^{-1}\mathcal{E})2\vartheta}{1 - \Upsilon^{-1}\vartheta} \right) \\ &\quad \times \Upsilon' \mathbf{U}_{N-1} \frac{\Upsilon^{-1}(\Upsilon - \vartheta)}{(\vartheta^2 - 1)} \\ &= \left( N(1 - \Upsilon^{-1}\vartheta) + \frac{1}{2} \Upsilon^{-1}\vartheta \right) \frac{\Upsilon'}{\mathbf{U}_{N-1}(\vartheta^2 - 1)}. \end{aligned} \tag{E.11}$$

Also

$$\begin{aligned} \widehat{\mathcal{D}} &= \mathbf{U}'_{N-2} \vartheta - \mathcal{P} \mathbf{U}'_{N-1} \vartheta - \mathcal{P}' \mathbf{U}_{N-1} \\ &= \left( ((\mathcal{P}^2 + 1 - 2\mathcal{P}\vartheta)N - (1 - \vartheta\mathcal{P})) \frac{\vartheta}{(\vartheta^2 - 1)} + \beta^{-1} \right) \mathbf{U}_{N-1} \\ &= 2\beta^{-1}\mathcal{E}(\mathcal{P} - \vartheta) \left( N - \frac{1}{2} \frac{(1 - \Upsilon\vartheta)}{(\beta^{-1}\mathcal{E})^2} \right) \frac{\mathbf{U}_{N-1} \beta^{-1} \beta^{-1} \mathcal{E} \Upsilon^{-1}}{(\vartheta^2 - 1)} \\ &= - \left( N - \frac{1}{2} \frac{(1 - \Upsilon\vartheta)}{(\beta^{-1}\mathcal{E})^2} \right) \frac{\beta^{-1} \beta^{-1} \mathcal{E} \Upsilon^{-1}}{\mathbf{U}_{N-1}(\vartheta^2 - 1)}, \end{aligned} \tag{E.12}$$

and

$$\mathcal{N} = (1 - \mathcal{P}^2) \mathbf{U}_{N-1}. \tag{E.13}$$

This is relevant for the transmission coefficient for the incident wave from the tubular side and also for the reflection coefficient for the incidence from ribbon. Then, by (E.1),

$$\hbar v(\xi, \mathcal{E}) = \frac{iz \widehat{\mathcal{D}}'(z, \mathcal{E})}{\widehat{\mathcal{D}}(z, \mathcal{E})}. \tag{E.14}$$

By (16),  $\overline{\vartheta(z_b, \mathcal{E})} = \vartheta(z_b, \mathcal{E})$  and using (E.2), and (E.3), (E.14) and (E.12),

$$\begin{aligned} \frac{\hbar v(\xi, \mathcal{E})}{\widehat{\mathcal{D}}'(z, \mathcal{E})} &= \frac{iz \widehat{\mathcal{D}}'(z, \mathcal{E})}{\widehat{\mathcal{D}}(z, \mathcal{E}) \widehat{\mathcal{D}}'(z, \mathcal{E})} = \frac{\Upsilon'(z_b)}{\Upsilon'(z_b)} \frac{iz}{\widehat{\mathcal{D}}(z, \mathcal{E})} \\ &= iz^{-1} \frac{1}{\left( N - \frac{1}{2} \frac{(1 - \Upsilon\vartheta)}{(\beta^{-1}\mathcal{E})^2} \right)} \frac{\mathbf{U}_{N-1}(\vartheta^2 - 1)}{\beta^{-1} \beta^{-1} \mathcal{E} \Upsilon^{-1}}, \end{aligned} \tag{E.15}$$

and

$$\begin{aligned} (-zz_P) \frac{\mathcal{N}(z, \mathcal{E}) \hbar v(\xi, \mathcal{E})}{\widehat{\mathcal{D}}'(z, \mathcal{E})} \\ = -iz_P \frac{(\vartheta^2 - 1)}{\left( N - \frac{1}{2} \frac{(1 - \Upsilon\vartheta)}{(\beta^{-1}\mathcal{E})^2} \right)} \frac{\Upsilon^2}{\beta^{-1}(\beta^{-1}\mathcal{E})^2}. \end{aligned} \tag{E.16}$$

Thus, in the context of (E.9),

$$\begin{aligned} \frac{|a^*(\kappa^i)_1|^2}{|a^*(\kappa_z)_N|^2} (-zz_P) \frac{\mathcal{N}(z) \hbar v}{\widehat{\mathcal{D}}'(z)} \\ = iz_P \frac{(\vartheta^2(z_P) - 1)}{N \beta^{-1} \mathcal{E} \beta^{-1}} \frac{1}{(1 - \mathcal{P}^2(z_P, \mathcal{E})) \Upsilon^{-1}(z_P)}. \end{aligned} \tag{E.17}$$

Note that (E.7) continues to hold. So (E.9) becomes

$$|\tau_{b\bar{a}}^{A\bar{A}}|^2 = \frac{1}{2} \widehat{C}_a \frac{z_{\bar{a}}}{(z_b - z_{\bar{a}})^2} \frac{\mathcal{N}_-(z_b) \widehat{\mathcal{D}}_+(z_b)}{\widehat{\mathcal{D}}_-(z_b) \mathcal{N}'_+(z_b)}, \tag{E.18}$$

where  $\widehat{C}_a$  is given by (52). Recall that for above expression, it was assumed that  $(1 - \mathcal{P}^2(z_a, \mathcal{E})) \neq 0, \mathbf{U}_{N-1}(\vartheta(z_a, \mathcal{E})) = 0$ .

0. Interestingly, though the detailed derivation is omitted, the same relation holds for the cases when  $(1 - \mathcal{P}^2(z_{\bar{a}}, \mathcal{E})) = 0$ ,  $U_{N-1}(\vartheta(z_{\bar{a}}, \mathcal{E})) \neq 0$  for the wave incidence from the tubular side and transmission into the ribbon. Hence, for all  $\mathbf{b}$  and  $\bar{\mathbf{a}}$ , it is found that (53) holds.

## References

1. S. Iijima et al., Nature **354**, 56 (1991)
2. N. Hamada, S.I. Sawada, A. Oshiyama, Phys. Rev. Lett. **68**, 1579 (1992)
3. Y. Kobayashi, K. Fukui, T. Enoki, K. Kusakabe, Y. Kaburagi, Phys. Rev. B **71**, 193406 (2005)
4. K.S. Novoselov, A.K. Geim, S.V. Morozov, D. Jiang, Y. Zhang, S.V. Dubonos, I.V. Grigorieva, A.A. Firsov, Science **306**, 666 (2004)
5. S.J. Tans, A.R. Verschueren, C. Dekker, Nature **393**, 49 (1998)
6. B. Trauzettel, D.V. Bulaev, D. Loss, G. Burkard, Nat. Phys. **3**, 192 (2007)
7. A.A. Balandin, Nat. Mater. **10**, 569 (2011)
8. M. Fujita, K. Wakabayashi, K. Nakada, K. Kusakabe, J. Phys. Soc. Jpn. **65**, 1920 (1996)
9. K. Nakada, M. Fujita, G. Dresselhaus, M.S. Dresselhaus, Phys. Rev. B **54**, 17954 (1996)
10. J.W. Wilder, L.C. Venema, A.G. Rinzler, R.E. Smalley, C. Dekker, Nature **391**, 59 (1998)
11. X. Jia et al., Science **323**, 1701 (2009)
12. M.C. Rechtsman, J.M. Zeuner, Y. Plotnik, Y. Lumer, D. Podolsky, F. Dreisow, S. Nolte, M. Segev, A. Szameit, Nature **496**, 196 (2013)
13. Y. Pennec, J.O. Vasseur, B. Djafari-Rouhani, L. Dobrzynski, P.A. Deymier, Surf. Sci. Rep. **65**, 229 (2010)
14. M. Polini, F. Guinea, M. Lewenstein, H.C. Manoharan, V. Pellegrini, Nat. Nanotechnol. **8**, 625 (2013)
15. R. Saito, G. Dresselhaus, M. Dresselhaus, *Physical properties of carbon nanotubes* (Imperial College Press, London, 1998)
16. N. Agrait, A.L. Yeyati, J.M. Van Ruitenbeek, Phys. Rep. **377**, 81 (2003)
17. M. Fuhrer et al., Science **288**, 494 (2000)
18. A. Bachtold, P. Hadley, T. Nakanishi, C. Dekker, Science **294**, 1317 (2001)
19. M.F. De Volder, S.H. Tawfick, R.H. Baughman, A.J. Hart, Science **339**, 535 (2013)
20. D.V. Kosynkin, A.L. Higginbotham, A. Sinitskii, J.R. Lomeda, A. Dimiev, B.K. Price, J.M. Tour, Nature **458**, 872 (2009)
21. L. Jiao, L. Zhang, X. Wang, G. Diankov, H. Dai, Nature **458**, 877 (2009)
22. A.L. Elías, A.R. Botello-Méndez, D. Meneses-Rodríguez, V. Jehová González, D. Ramírez-González, L. Ci, E. Muñoz-Sandoval, P.M. Ajayan, H. Terrones, M. Terrones, Nano Lett. **10**, 366 (2009)
23. A. Cano-Márquez, F. Rodríguez-Macías, J. Campos-Delgado, C. Espinosa-González, F. Tristán-López, D. Ramírez-González, D. Cullen, D. Smith, M. Terrones, Y. Vega-Cantú, Nano Lett. **9**, 1527 (2009)
24. Y. Yoon, S. Salahuddin, Appl. Phys. Lett. **97**, 033102 (2010)
25. S. Costamagna, A. Schulz, L. Covaci, F. Peeters, Appl. Phys. Lett. **100**, 232104 (2012)
26. J.S. Friedman, A. Girdhar, R.M. Gelfand, G. Memik, H. Mohseni, A. Taflove, B.W. Wessels, J.P. Leburton, A.V. Sahakian, Nat. Commun. **8**, 15635 (2017)
27. H. Santos, L. Chico, L. Brey, Phys. Rev. Lett. **103**, 086801 (2009)
28. Y.O. Klymenko, Eur. Phys. J. B **77**, 433 (2010)
29. L. Chico, H. Santos, A. Ayuela, W. Jaskólski, M. Pelc, L. Brey, Acta Phys. Pol. A **118**, 433 (2010)
30. K.L. Ma, X.H. Yan, Y.D. Guo, Y. Xiao, Eur. Phys. J. B **83**, 487 (2011)
31. B.L. Sharma, Z. Angew. Math. Phys. **69**, 16 (2018)
32. J.B. David, K. Ferry, S.M. Goodnick, *Transport in nanostructures*, 2nd edn. (Cambridge University Press, Cambridge, UK, 2009)
33. M. Brandbyge, M.R. Sørensen, K.W. Jacobsen, Phys. Rev. B **56**, 14956 (1997)
34. M. Brandbyge, J.L. Mozos, P. Ordejón, J. Taylor, K. Stokbro, Phys. Rev. B **65**, 165401 (2002)
35. P.R. Wallace, Phys. Rev. **71**, 622 (1947)
36. J. Callaway, *Energy band theory*, in Pure and applied physics (Academic Press, New York, 1964)
37. E. Hückel, Z. Phys. **60**, 423 (1930)
38. R. Mittra, Y.L. Hou, V. Jamnejad, IEEE Trans. Microw. Theory Tech. **28**, 36 (1980)
39. J.T. Londergan, J.P. Carini, D.P. Murdock, *Binding and scattering in two-dimensional systems: applications to quantum wires, waveguides, and photonic crystals*, 1st edn. Lecture notes in physics monographs, (Springer, Berlin, Heidelberg, 2000)
40. S. Datta, in *Electronic transport in mesoscopic systems*. Cambridge studies in semiconductor physics and microelectronic engineering (Cambridge University Press, Cambridge, UK, 1995), Vol. 3
41. B. Noble, *Methods based on the Wiener-Hopf technique* (Pergamon Press, London, 1958)
42. B.L. Sharma, Z. Angew. Math. Phys. **66**, 3591 (2015)
43. R. Landauer, IBM J. Res. Dev. **1**, 223 (1957)
44. R. Landauer, Phys. Scripta **1992**, 110 (1992)
45. C. Hamaguchi, *Quantum structures* (Springer, Berlin, Heidelberg, 2001), p. 307
46. P.L. Chebyshev, Mém. Acad. Sci. Pétersb. **7**, 539 (1854)
47. J.C. Mason, D.C. Handscomb, *Chebyshev polynomials* (Chapman & Hall/CRC, Boca Raton, FL, 2003)
48. N. Cortés, L. Chico, M. Pacheco, L. Rosales, P. Orellana, EPL **108**, 46008 (2014)
49. P. Orellana, L. Rosales, L. Chico, M. Pacheco, J. Appl. Phys. **113**, 213710 (2013)
50. B.L. Sharma, Waves Random Complex Media **28**, 96 (2018)
51. A. Weisshaar, J. Lary, S.M. Goodnick, V.K. Tripathi, J. Appl. Phys. **70**, 355 (1991)
52. W.D. Sheng, J. Phys. Condens. Matter **9**, 8369 (1997)
53. B.L. Sharma, Wave Motion **65**, 55 (2016)
54. B.L. Sharma, Wave Motion **59**, 52 (2015)
55. B.L. Sharma, Z. Angew. Math. Phys. **66**, 2719 (2015)
56. K. Yates, *Hückel molecular orbital theory* (Academic Press, New York, 1978)
57. E. Economou, *Green's functions in quantum physics* (Springer, Heidelberg, 1979)
58. B.L. Sharma, Int. J. Solids Struct. **80**, 465 (2016)

59. M.J. Ablowitz, A.S. Fokas, *Complex variables: introduction and applications* (Cambridge University Press, Cambridge, UK, New York, 1997)
60. A. Weisshaar, J. Lary, S. Goodnick, V. Tripathi, Appl. Phys. Lett. **55**, 2114 (1989)
61. K. Wakabayashi, Y. Takane, M. Yamamoto, M. Sigrist, Carbon **47**, 124 (2009)
62. B.L. Sharma, SIAM J. Appl. Math. **76**, 1355 (2016)
63. T. Wehling, A.M. Black-Schaffer, A.V. Balatsky, Adv. Phys. **63**, 1 (2014)
64. Y. Kobayashi, K. Fukui, T. Enoki, K. Kusakabe, Phys. Rev. B **73**, 125415 (2006)
65. B. Wang, J. Wang, Phys. Rev. B **81**, 045425 (2010)
66. Y.W. Son, M.L. Cohen, S.G. Louie, Phys. Rev. Lett. **97**, 216803 (2006)
67. L. Yang, C.H. Park, Y.W. Son, M.L. Cohen, S.G. Louie, Phys. Rev. Lett. **99**, 186801 (2007)
68. Y.V. Nazarov, *Quantum transport: introduction to nanoscience*, 1st edn. (Cambridge University Press, Cambridge, UK, 2009)
69. F.A. Buot, Phys. Rep. **234**, 73 (1993)
70. T. Ihn, in *Electronic quantum transport in mesoscopic semiconductor structures*, 1st edn. Springer tracts in modern physics, (Springer-Verlag, New York, 2004), Vol. 192
71. D.A. Wharam, T.J. Thornton, R. Newbury, M. Pepper, H. Ahmed, J.E.F. Frost, D.G. Hasko, D.C. Peacock, D.A. Ritchie, G.A.C. Jones, J. Phys. C: Solid State Phys. **21**, L209 (1988)
72. B.J. van Wees, H. van Houten, C.W.J. Beenakker, J.G. Williamson, L.P. Kouwenhoven, D. van der Marel, C.T. Foxon, Phys. Rev. Lett. **60**, 848 (1988)
73. J. Park, G. He, R.M. Feenstra, A.P. Li, Nano Lett. **13**, 3269 (2013)
74. R. Egger, A.O. Gogolin, Phys. Rev. Lett. **79**, 5082 (1997)
75. C. Kane, L. Balents, M.P.A. Fisher, Phys. Rev. Lett. **79**, 5086 (1997)
76. A.R. Hernández, C.H. Lewenkopf, Phys. Rev. B **86**, 155439 (2012)
77. J. Tworzydło, C. Groth, C. Beenakker, Phys. Rev. B **78**, 235438 (2008)
78. L.I. Slepyan, *Models and phenomena in fracture mechanics* (Springer, New York, Berlin, Heidelberg, 2002)
79. B.L. Sharma, SIAM J. Appl. Math. **75**, 1171 (2015)
80. B.L. Sharma, Sādhanā **42**, 901 (2017)
81. N. Wiener, E. Hopf, Sitzungsber. Preuss. Akad. Wiss. Berl. Phys. Math. **32**, 696 (1931)
82. I. Singer, E. Turkel, J. Comput. Phys. **201**, 439 (2004)
83. J.P. Berenger, J. Comput. Phys. **114**, 185 (1994)